Commandable Cut-Down and Tracking Instrument for Lightning Research, and Correlation Study Between Lightning Flash Counts and Meteorological Parameters

by

William Walden-Newman

Submitted in Partial Fulfillment

of the Requirements for the Degree of

Master of Science in Physics

New Mexico Institute of Mining and Technology

Socorro, New Mexico

May, 2008

ABSTRACT

Two methods were developed to improve balloon-borne lightning research carried out at Langmuir Laboratory. First, a commandable cut-down and tracking instrument was developed for lightning research in tropospheric and near-space environments to remotely detach balloon payloads lifted into active thunderstorms. The instrument is designed to melt monofilament by heating a nichrome wire using a 9 V battery, and to utilize the Automatic Position Reporting System for telemetry up to a distance of 60 km from a station. The instrument was used successfully to retrieve electric field sondes during the summer of 2007.

Second, a correlation study was conducted by comparing data collected by the Los Alamos Sferic Array, containing total lightning flash counts from the summer months of 2005 and 2006, and corresponding data from upper air balloon soundings at National Weather Service stations. Correlation coefficients were determined between the number of flashes, the mixing ratio of water vapor to air, convective available potential energy, air temperature, and wind speed at ground level and 500 hPa. The results show that the mixing ratio has a strong correlation with flash count in the Southwestern U.S. and can be used to predict afternoon thunderstorms.

ACKNOWLEDGMENT

I would like to thank Dr. Richard Sonnenfeld for his constant advice and assistance throughout my graduate program. He went out of his way to point me in the right directions for my research, as well as offer valuable tips on how to succeed in science. I thank Dr. Kenneth Eack for his wonderful assistance on understanding the instrument and for giving me the insight on how to solve the challenging problem concerning the instrument's radio. I thank Dr. David Raymond for his clear explanations on atmospheric physics that greatly assisted me with the correlation study.

I thank Dr. Carlos Lopez Carrillo for explanations on atmospheric convection and CAPE, as well as Norton Euart for advice on design aspects of the instrument. I thank the faculty of the physics department for doing a great job at teaching and keeping my interest in the subject. I thank the NSF for additional funding through grant ATM-0331164 and the NASA Space Grant Program for financial support, as well as Xuan Min Shao and Mike Stock of Los Alamos for providing LASA data used in the correlation study. I also thank Dr. William Winn and the staff of Langmuir Laboratory for allowing me to conduct my research.

Lastly, I thank Erica Jane Knee, my family, and the many close friends I have met in college for their constant encouragement throughout my education, especially my grandfather for introducing me to calculus and computers at an age much too early.

This thesis was typeset with LaTeX[1] by the author.

[1] LaTeX document preparation system was developed by Leslie Lamport as a special version of Donald Knuth's TeX program for computer typesetting. TeX is a trademark of the American Mathematical Society. The LaTeX macro package for the New Mexico Institute of Mining and Technology thesis format was adapted from Gerald Arnold's modification of the LaTeX macro package for The University of Texas at Austin by Khe-Sing The.

TABLE OF CONTENTS

LIST OF TABLES

LIST OF FIGURES

This thesis is accepted on behalf of the faculty of the Institute by the following committee:

Richard G. Sonnenfeld,Advisor

William Walden-Newman | Date

PREFACE

In scientific research, one often works on what goes unpublished and publishes on what works. I was fortunate at New Mexico Tech that two projects worked, both of which address challenges for research in atmospheric electrification, storm prediction, and reliable instrument recovery. Accordingly, this document has two main sections that stand independently. The first is a discussion of an improved scientific payload recovery and tracking instrument for balloon applications, while the second reports a relatively simple and promising way to predict summer-afternoon storms in the southwestern United States. Appendices include a glossary of abbreviated terms, a parts list, schematics and photos of the instrument, code for programming several devices, code for calculating meteorological parameters, and the results of a range test.

William Walden-Newman

New Mexico Institute of Mining and Technology

May, 2008

CHAPTER 1

Introduction to the Instrument

1.1 Goals and Capabilities of the Command Cut-down Instrument

I sought to develop a commandable cut-down and tracking instrument for thunderstorm research. This instrument allows for easier retrieval of balloon-borne scientific payloads by causing them to descend as soon as their scientific objective is complete. It disconnects a scientific payload attached to a balloon either remotely by command or with a calibrated timer/pressure sensor by melting the monofilament balloon tether. This helps field researchers perform various types of ballooning experiments on atmospheric phenomena, including the difficult process of launching multiple electric field sondes (E-sondes) into the same thunderstorm. The results of that experiment will lead to the best understanding of charge motion within intra-cloud (IC) and cloud-to-ground (CG) lightning channels (Sonnenfeld, 2006; Hager, 2007).

In addition to cut-down, the instrument also acts as an independent telemetry system, allowing for easier development of new instruments for sci-

Functions	Independent telemetry/cut-down system
Retrieval method	Safe and reliable
Weight	Less than 6 pounds
Transmission range	At least 50 km
Battery life	At least 48 hours

Table 1.1: Instrument Requirements

entific micro-ballooning research. Since the problem of recovery is solved, more focus can be put to the specific scientific objective of the instrument being flown. The current cut-down instrument can transmit position and velocity data to an Automatic Position Reporting System (APRS) station up to a distance of 60 km. APRS is a system of repeater stations that operate in the amateur radio bands. The instrument also has an extended battery life that allows for retrieval several days after flight. The search could include using ground vehicles or aircraft to receive a transmission from the instrument while its on the ground.

1.2 A Comparison to Prior Cut-down Instruments

Although the instrument reported here has a unique set of capabilities for balloon-borne research, cut-down devices have previously been built and used. The first remote cut-down system was built by General Mills in the early 1950's. It was used in high-altitude balloon flights under the experiment named project Gopher, conducted by Charles B. Moore of General Mills in conjunction with the U.S. Air Force (Parsch, 2006). They cut monofilament using a squib, or small explosive, triggered by a timer or radio command. Though Gopher's cut-down device detached instrument payloads from a polyethylene balloon, it did not have a tracking function. Other types of cutting mechanisms have been developed in later instruments, including a B-field sensor used by the University of Wisconsin and the National Center for Atmospheric Research (NCAR) (Levanon et al., 1975), but these are not remotely controlled. The B-field sensor is connected to a counter that heats a resistor wrapped around monofilament once the B-field has reached a set value for more than 30 seconds

(Levanon et al., 1975).

Several remote cut-down instruments were developed by sources ranging from amateur balloonists (Meehan, 2002) to various meteorological organizations that include NCAR and the National Scientific Balloon Facility (NSBF). The instrument patented by NCAR includes not only a remote cut-down mechanism and tracking system, but also an aerodynamic housing to guide the instrument payload to a designated landing site after its detachment from the balloon (Lauritsen, 1991). The device is also equipped with an aircraft rudder to adjust its flight path. However, the exterior is composed of styrofoam, leaving the electronics vulnerable to corona discharge in a thunderstorm. The instrument developed at NSBF has both remote cut-down and tracking capabilities, but relies on ground telemetry maintained by NSBF that is only near launch sites (Farman, 1999).

My instrument maintains the twin capabilities of remote cut-down and tracking, while avoiding the design and infrastructure requirements of the prior instruments. Instead of using squibs, with the chance of accidental discharge on the ground upon retrieval, this device has a thermal cutting mechanism that poses little threat. It also maintains a compact size ($<$ 6 pounds) and low cost (approximately \$ 500) for micro-ballooning experiments and takes advantage of a nation-wide repeater system. In this case, the system is APRS and requires an amateur radio license. The instrument also has a metal housing to protect the electronics from corona discharge.

CHAPTER 2

Instrument Hardware

2.1 System Description

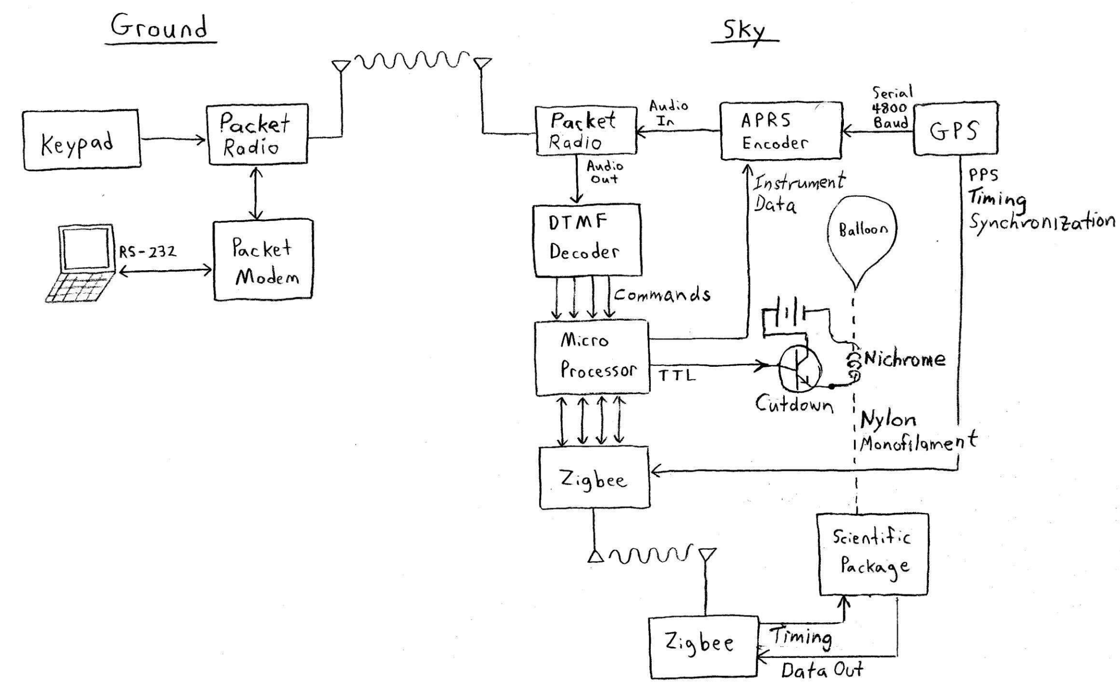

Figure 2.1: Command cut-down block diagram: Illustrates both the ground and sky based system components. The Zigbees were not implemented and represent a future addition.

A summary of the functionality and architecture of the command cut-down system is shown Fig. 2.1. There are two components of the system with one at ground level and the other aloft. On the ground is a computer station with mapping software, packet modem, and radio, that receives global positioning system (GPS) data from the cut-down instrument and transmits a cut command. During flight, the instrument encodes data from a GPS^{B1} unit with an APRS encoder called a Tinytrak^{B2} and transmits position data with a VX-2 radio^{B3} at the APRS frequency 144.39 MHz.[1] The APRS repeater system posts information on the world-wide-web that includes the instrument's position overlayed on terrain data from Google Earth as well as weather radar from Nexrad. This is shown below in Fig.'s 2.2 and 2.3. The Zigbees are low powered radios and were not implemented in this design. They represent possible future enhancement of the instrument as a full experiment controller.

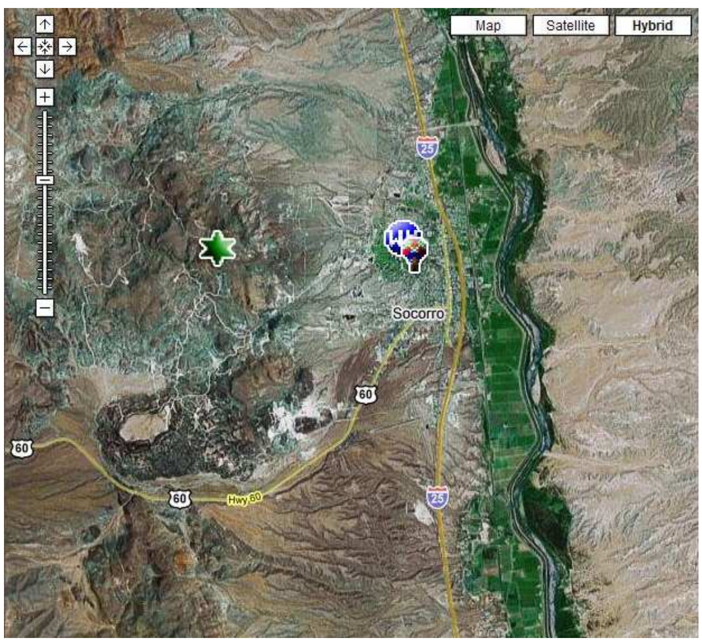

Figure 2.2: Map from www.openaprs.net: instrument location (balloon), local APRS stations (star and WX), roads, and ground terrain.

[1]Superscripts indicate the reference number for each part in Appendix B.

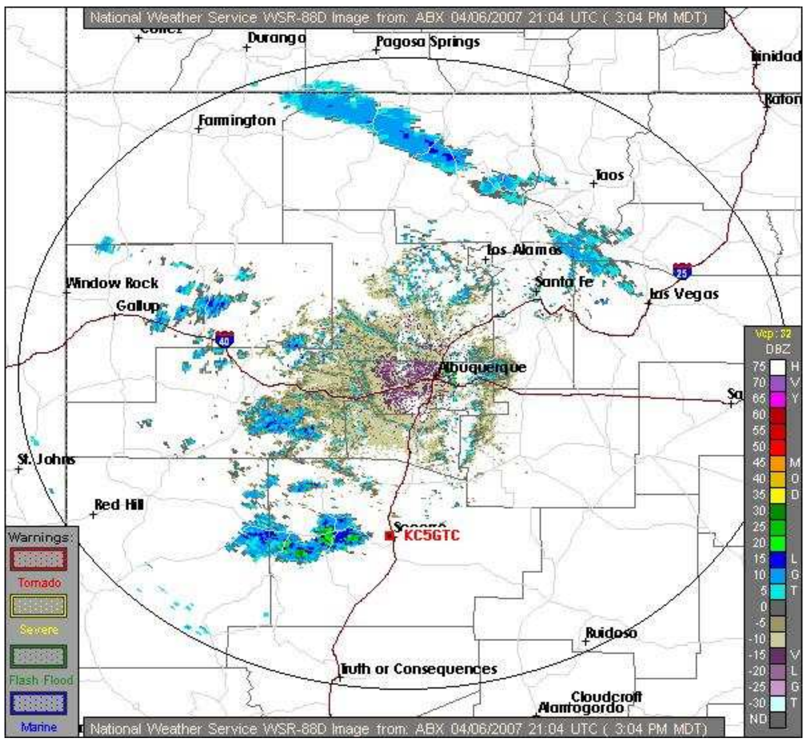

Figure 2.3: Map from www.findu.com: instrument location (red square), instrument name (KC5GTC), and local radar.

As mentioned before, cut-down is activated by a radio command and is sent via a touch tone keypad on the ground at 148.95 MHz, one of Langmuir Lab's licensed frequencies. The command is received by the VX-2 on the instrument, which relays the audio signal to a dual-tone multi-frequency (DTMF) decoder[B4] on a cut-down circuit. Cut-down commands are converted by the DTMF decoder to a 4-bit binary code which is sent to a programmable intelligent computer (PIC) microcontroller[B5]. The string is analyzed to see if it matches the stored cut-down code, and if so, the PIC sends a transistor-transistor logic (TTL) high level to an silicon controlled rectifier[B6] (SCR). This shorts a 9 V battery[B7] to ground, drawing a current of approximately 3 A across the SCR to a nichrome wire wrapped around monofilament causing it to melt.

The cut-down instrument is part of a balloon chain shown in Fig. 2.4 consisting of a scientific payload, a damper to keep the payload from swinging, a detangler ring to prevent the parachute lines from tangling, a nylon parachute, the cut-down instrument, and finally a latex helium balloon. The instrument is connected to the balloon by a strand of 180 lb test monofilament[B8] through a hole in the middle of the parachute. This strand is cut upon command cut-down. Another strand is connected from the instrument to the central detangler ring, to keep the cut-down instrument attached to the rest of the chain after cut-down. The rest of the chain is only connected to the detangler ring.

2.2 Cut-down Instrument External Layout

Other than system functionality, a lot of time was spent on finding ways to handle the difficulties of foul weather balloon flights in lightning research. For example, the outer casing shown in Fig. 2.5 is designed to prevent

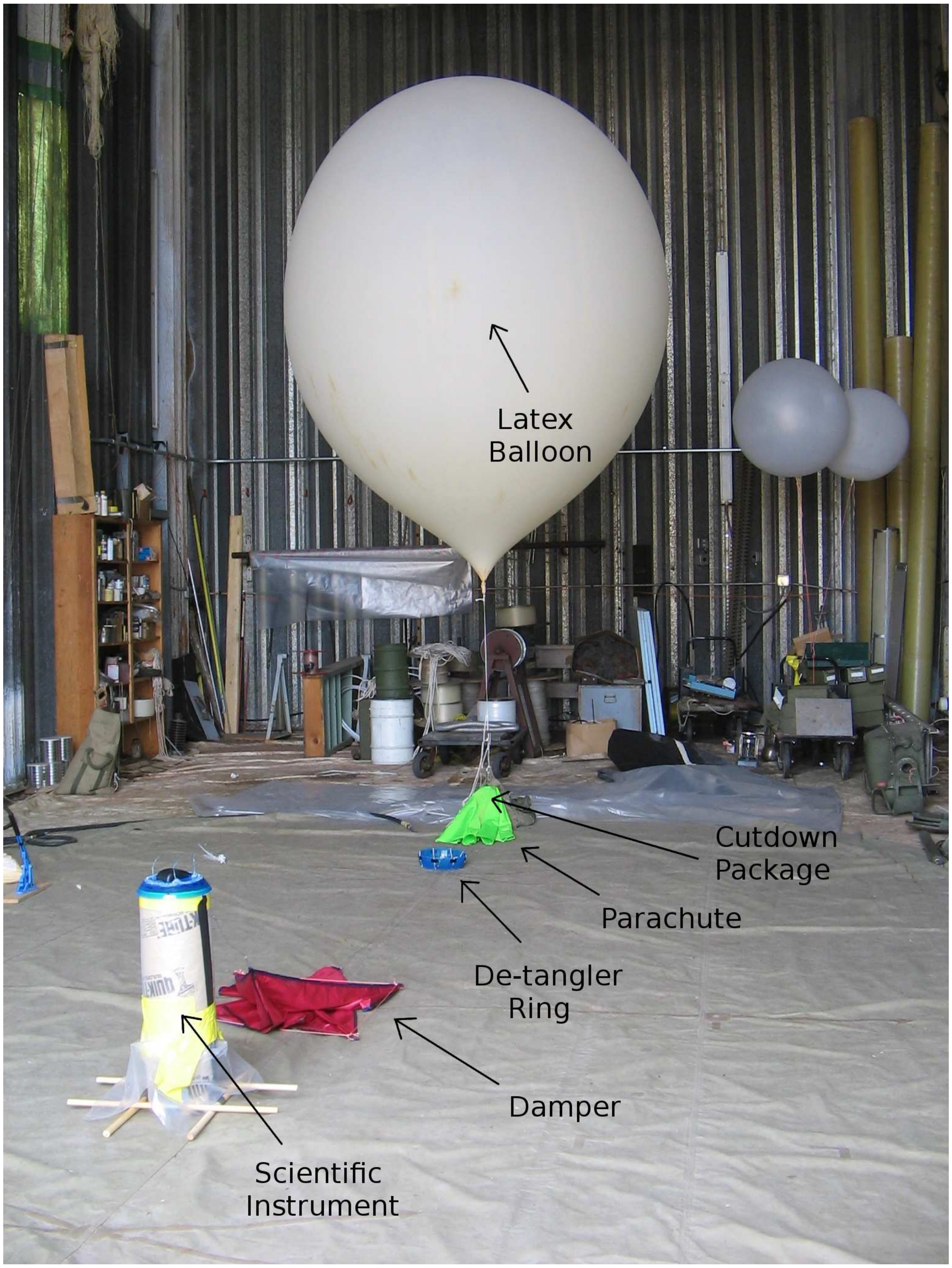

Figure 2.4: Balloon Chain: Illustrates the various components.

corona discharge from harming or interfering with the instrument's electronics while inside a thunderstorm, and is composed of three different parts. The side of the cylinder is made of aluminum[B9] and is held together at the top by a 1" x 6" cake pan[B10], and at the bottom by a 1" x 5" cake pan. A schematic of this part, as well as others, is shown in Appendix C. Fig. 2.5 also shows the antenna below the instrument and GPS receiver mounted at the top. There are also two loops of monofilament attached to the lid that can connect to a balloon.

The bottom cake pan shown in Fig. 2.6 has a 3.75" diameter hole cut in the center, so that the bottom board[B11] of the inside structure can be exposed. The bottom pan is permanently attached to the sides, while the top is attached with hex bolts and can be removed. The bottom of the instrument contains several mounted parts, including a light-emitting diode[B12] (LED) that indicates whether the timer and counter chips are working on the cut-down circuit. Below the LED is a female-to-female (F/F) bulkhead adapter[B13] that the antenna connects to. Above the LED is a 0.25" hole for the monofilament to pass through the instrument, which is lined with a rubber grommet[B14] to protect the monofilament from scraping against aluminum during flight. To the right of the LED is a toggle for the power control switch[B15]. Four threaded, metal spacers surround the bottom board and attach it to the outer casing with another set of spacers taped inside.

2.3 Cut-down Instrument Internal Layout

While the outside of the instrument is optimized for corona protection, the inside is organized to minimize noise on the cut-down circuit from the radio.

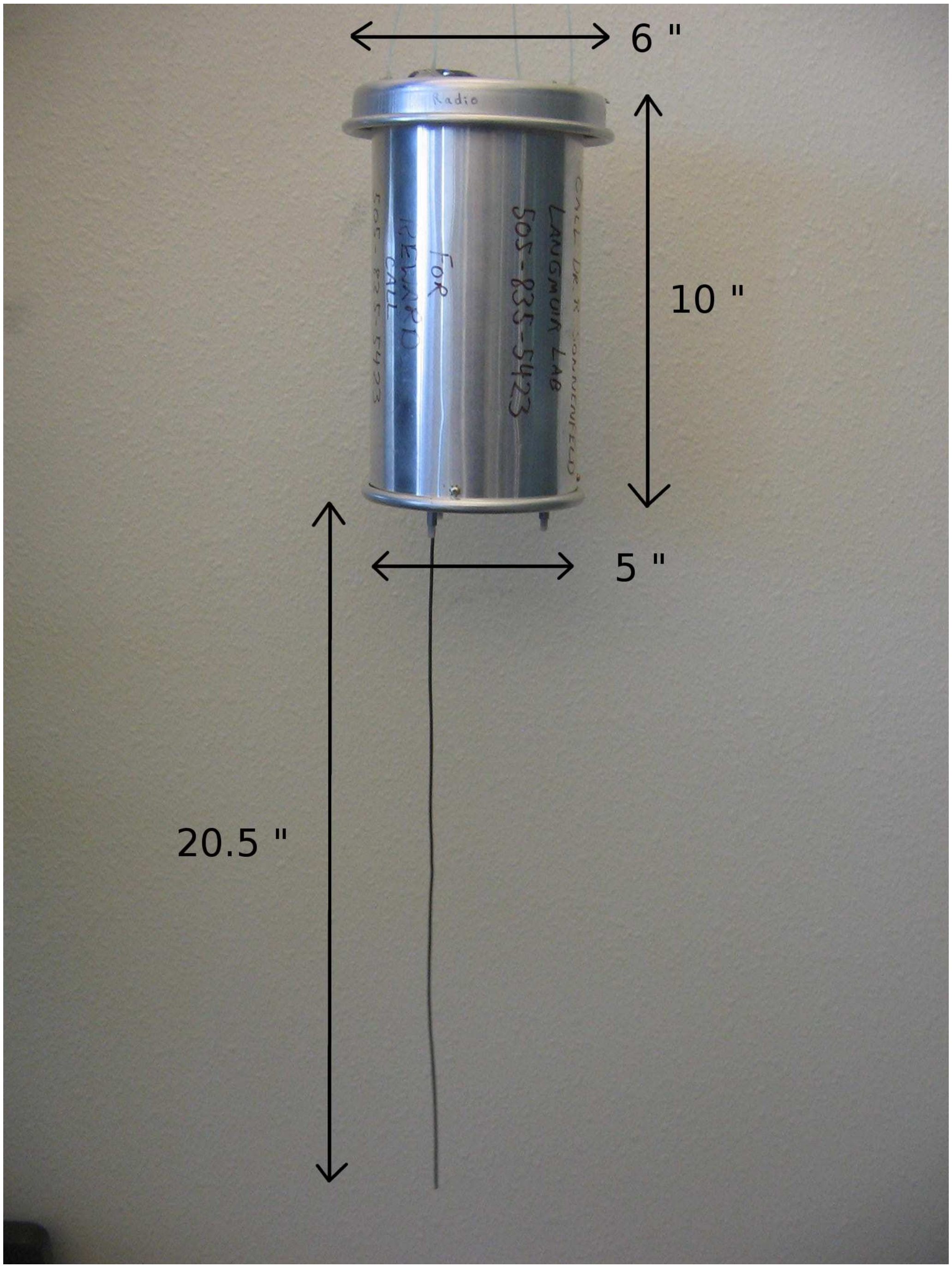

Figure 2.5: Cut-down Instrument: Shows actual dimensions.

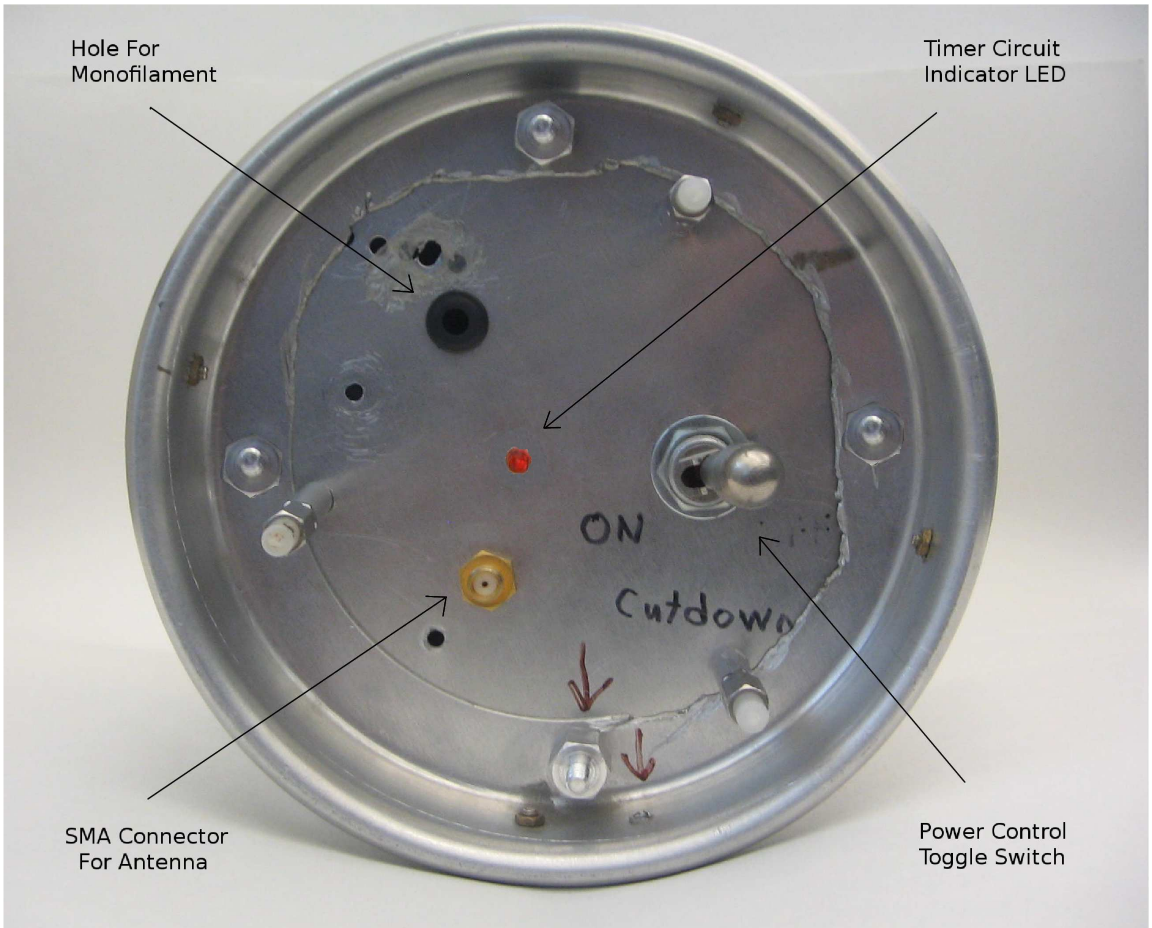

Figure 2.6: Bottom of Instrument: When the switch is thrown, the LED flashes for every count of the timer counter circuit.

This is accomplished by separating the radio and circuit into two levels with an aluminum plate, as shown in Fig. 2.7. All levels are held together with three 4-40 all-thread posts[B16] that are covered with plastic spacers[B17]. On the bottom half of the instrument, the radio is taped to a post with filament tape, and next to it is the toggle switch mounted with screws. Battery packs 3 and 4 are not installed in Fig. 2.7, but would normally be taped to the bottom plate inside the instrument. Other views of inside the instrument are shown in Appendix D.

On the top half is the cut-down circuit with battery packs 1 and 2 taped to the aluminum plate. Behind the battery packs, and not visible from Fig. 2.7, is the GPS unit mounted sideways to a post. Above these parts are two acrylic plates[B20] that house the pressure sensor. It consists of a small brass screw mounted to the top plate and a pressure bellows mounted on the bottom. The center of the bellows is aligned with the screw. The brass tubes of the cut-down circuit pass through holes in both the aluminum and acrylic plates to hold it in place. Both holes are aligned with rubber grommets on the top and bottom, allowing monofilament to pass through the entire instrument.

2.4 Cut-down Circuit

The cut-down circuit controls when the remote or timer/pressure cut-down activates. The circuit board is shown in Fig. 2.8, along with a board trace and schematic in Appendix E. The cut-down works by heating up the small nichrome wire wrapped around monofilament shown in Fig. 2.9. It is attached at each end to a small screw that goes through the circuit board. The monofilament divides the circuit into two halves, one corresponding to the

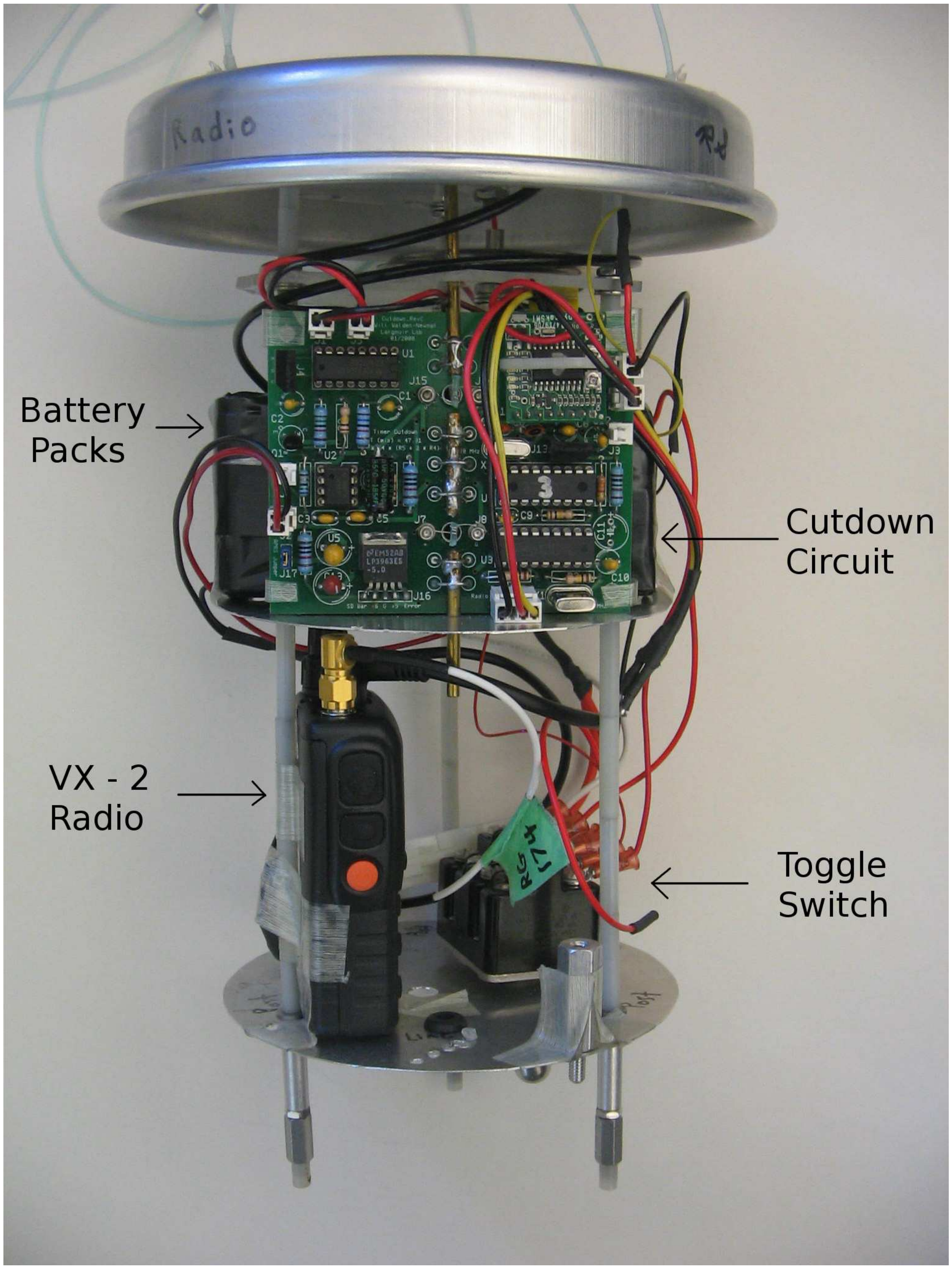

Figure 2.7: Inside cut-down instrument: Shows the front view.

remote cut-down and one to the timer/pressure cut-down. Each side is fully redundant, acting as independent cut-down methods, with its own nichrome wire and a corresponding 9 V battery inside the instrument.

The timer/pressure cut-down consists of a 555 timer[B21], 13-bit counter[B22], transistor[B23], SCR, LED outside the instrument, and a connector[B24] to the pressure bellows. When the instrument is turned on, it begins a timer that counts by an RC time constant that is configured within the circuit. For every time constant, the counter adds 1 until it reach 2^{12} times RC. At this time, the counter sends a TTL high level to the SCR, which dumps current across the nichrome. The LED is connected to an output pin on the transistor, and blinks every time constant. At lower pressures, the bellows will expand vertically. If the top of the bellows and the screw above it touch, it shorts two wires coming from each part that are connected across a 9 V battery and the nichrome wire by way of a connector on the circuit. This also dumps a large amount of current across the nichrome.

2.5 Tinytrak/APRS

On the cut-down circuit is the Tinytrak, which controls the radio's transmission rate. I used the Tinytrak programmer to include a balloon symbol and a transmission rate of once every 2 minutes, which is the fastest rate recommended for amateur radio bands (Kenneth Eack, New Mexico Tech, keack@nmt.edu, private communication). A list of device specifications is shown in Table 2.1. The Tinytrak is mounted on the circuit in a removable fashion. Small metal posts are soldered through its output pads which are then connected to a female connector soldered to the circuit. Cable ties go through

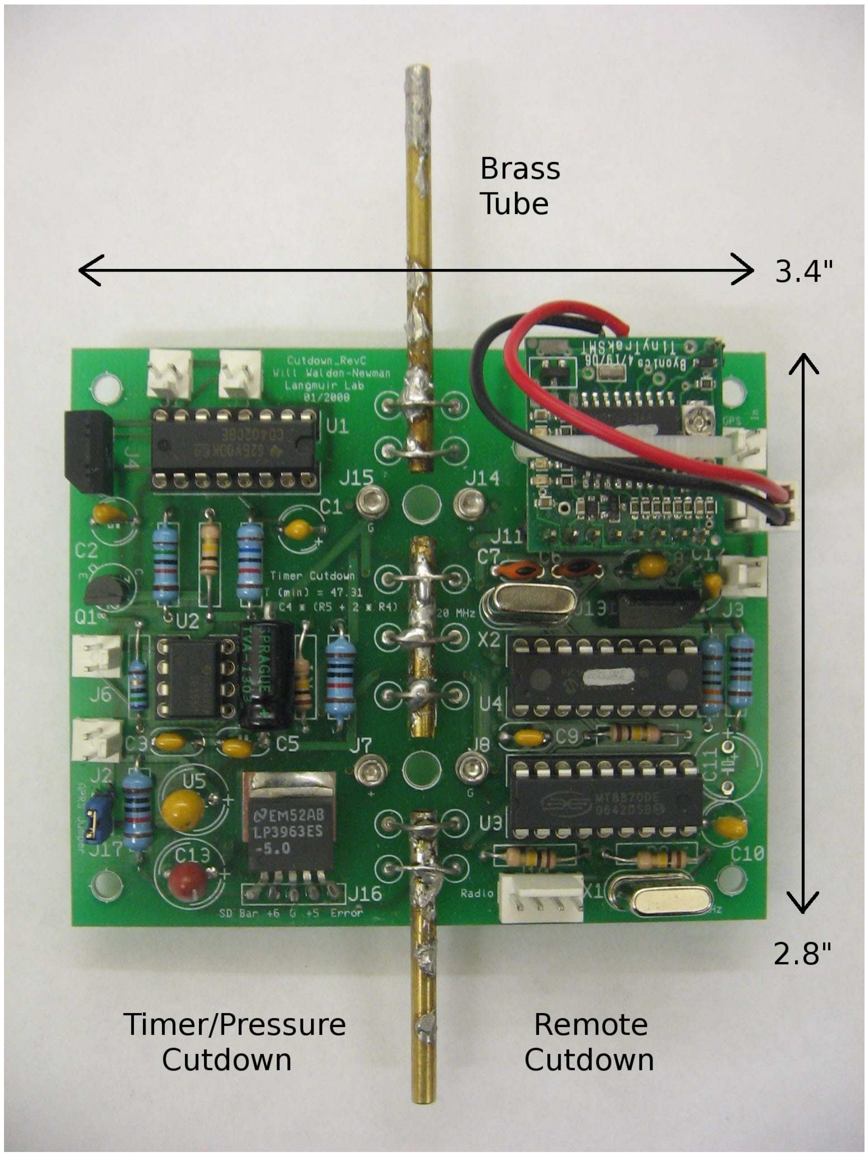

Figure 2.8: Cut-down Circuit: Illustrates that each side of the circuit constitutes a different cut-down mechanism.

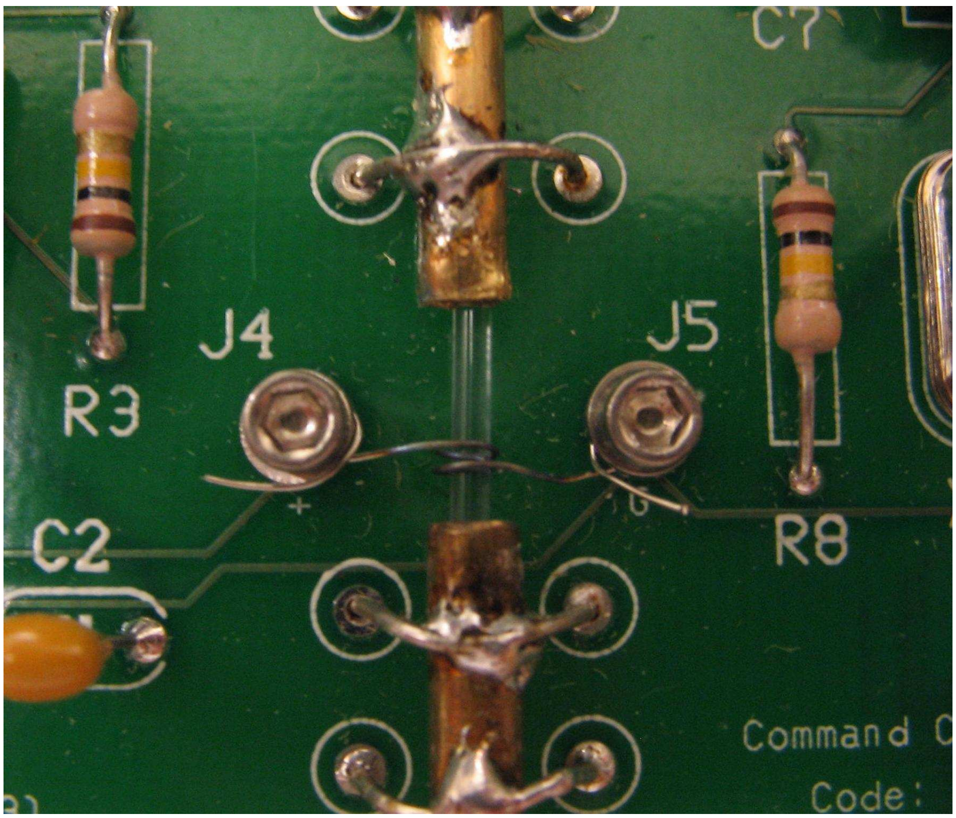

Figure 2.9: Nichrome Wire: Wraps 3 times around the monofilament, and around a screw at each end.

Weight	2.8 g
Size	1” (w) x 0.925” (l) x 0.16” (h)
Tested Operating Temp.	0 ^{o}C to 49 ^{o}C
Input Voltage	8 VDC to 18 VDC
Maximum Current Draw	20 mA
Transmit Data Rate	1200 baud
GPS Data Rate	4800 baud

Table 2.1: Tinytrak Specifications (Garrabrant, 2008)

two holes on the circuit and then around the Tinytrak to keep it rigidly held during flights.

Both surfaces of the Tinytrak, shown in Fig.'s 2.10 and 2.11, are used in operation. Power is applied directly to pad 1 (Power In) and pad 2 (Ground) on the top surface of the Tinytrak. A toggle was configured using the bottom surface to allow a single transmission on command. By programming the PIC to lower pin 8 for 0.2 seconds when the correct toggle command is sent, pin RB6 is shorted to GND. This causes the Tinytrak to briefly switch from transmit mode B to A, causing a single transmission. The connector J8 on the cut-down circuit links the PIC to pads RB6 and GND on the Tinytrak. The capacitor C11 (referenced from Fig. 2 in Appendix E) was initially added to prevent the Tinytrak from locking in Mode A, but later testing showed that the instrument can function without it.

2.6 Radio

The Tinytrak encodes GPS data that is eventually transmitted by a VX-2, or VX-3, radio. A list of device specifications for the radio is shown in Table 2.2. In order to extend power lifetime, I removed the original rechargeable

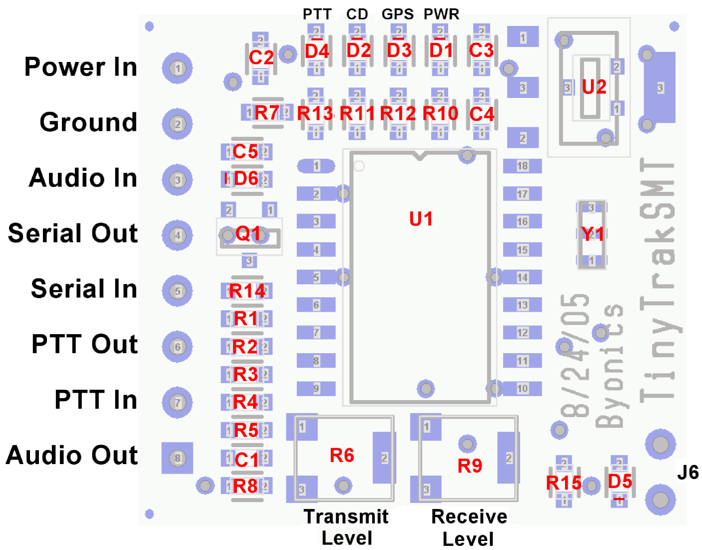

Figure 2.10: Output pins on the top surface of Tinytrak (Garrabrant, 2008)

Figure 2.11: Output pins on the bottom surface of Tinytrak (Garrabrant, 2008)

Weight	132.0 g
Size	47 mm(w) x 23 mm (l) x 81 mm (h)
Operating Temperature	-20^{o}C to +60^{o}C
Input Voltage	5.5 VDC to 7 VDC
Current Draw	150 mA (Receive), 1.8 A (Transmit at 144 MHz and 6.0 V)
RF Power Output	3 W (At 144 MHz and 6.0 V)
Antenna Impedance	50 Ω
RX Frequency Range	0.5 to 999 MHz
TX Frequency Range	144 to 146 MHz, and 430 to 440 MHz

Table 2.2: Radio Specifications (Vertex Standard, 2003)

battery, replaced the cover, and applied power to the external power connector marked 'Ext Vdc'. This extended the operation time from 9 hours to 2 days. The custom-built antenna mounted outside the bottom board is attached to the radio using an RG-174 SMA cable[B25], and a connector[B26] for audio in/out attaches from the radio to the cut-down circuit. Instructions for programming the radio to transmit and receive at different frequencies are in Appendix F.

2.7 GPS

The GPS sends two types of output strings every second to the Tinytrak. GPRMC displays the latitude, longitude, course, and speed, while GPGGA displays latitude, longitude, altitude, and descent rate. A sample of output data is shown below, with data listed in the following order: time (hour, minute, seconds), latitude (degrees, decimal minutes), longitude, heading or course (degrees from North), speed, altitude, and instrument number. The instrument number is a programmable string in the Tinytrak. In addition to the GPS unit, a receiving antenna is mounted on the top lid and is built with a plastic cover to handle water and hail. Device specifications are shown

Weight	15.0 g
Size	35.56 mm(w) x 45.85 mm (l) x 8.31 mm (h)
Operating Temperature	-30^{o}C to +80^{o}C
Input Voltage	8.0 VDC to 40 VDC unregulated
Current Draw	50 mA nominal 60 mA peak
Satellite Tracking	12
Position Update Rate	1 sec.
Acquisition Time	45 sec. cold to 5 min. sky search
Position Accuracy	15 m
Interface	RS-232 compatible with baud 300 to 38400
Data Format	NMEA 0183 ver. 2.0 and 3.00

Table 2.3: GPS Specifications (Garmin International, 2006)

in Table 2.3.

```
Sample of GPS Output Data:

/182620h3358.57N/10712.84W0282/015/A=020773/W07-01

Key:
Time / Lat. / Long. / Dir. / Speed / Alt. / Instrument No.
```

2.8 Batteries

The GPS and other devices have specific types of batteries to serve their various functions. Lithium type batteries were chosen for the 6 and 18 V supplies because they perform better at low temperatures, as well as last up to 3 times longer than alkaline batteries at low current draw. Alkaline 9 V batteries performed better at transferring high currents during cut-down tests. Thus, one is used for each type of cut-down mechanism. In addition, the Alkaline used for the Timer/Pressure cut-down also powers the counter and timer chips. The counter is typically set for 2^{12} counts, corresponding to a 50

Battery Pack	1	2	3 and 4
Chemistry Type	Lithium	Alkaline	Lithium
Battery	AA	9 V	9 V
Batteries in series	4	2	1
Batteries in parallel	3	2	1
Battery Pack Voltage	6 V	18 V	9 V
Weight of pack	174 g	135.2 g	45.6 g
Operating Temp.	-40^{o}C to +60^{o}C	-40^{o}C to +60^{o}C	-18^{o}C to 55^{o}C
Capacity	3000 mAh	1200 mAh	600 mAh

Table 2.4: Battery Pack Specifications (Energizer, 2008)

minute time limit, that uses only 0.07 % of the battery's energy leaving most to drain on the nichrome wire.

A summary of each battery pack and specifications is shown in Table 2.4. Assuming the capacities given, all devices in the cut-down instrument should last a minimum of 48 hours, with the GPS being the first device to power down. Thus, location data will be present throughout the flight and the radio will continue to transmit for two days on the ground.

2.9 Switch

In addition to specialized batteries, I chose a military-grade locking-toggle switch. It has 4-poles to satisfy voltages for each of the battery packs, and the locking toggle prevents accidental switching at take-off by the person holding the instrument. Past ballooning instruments have shown that solder can melt the plastic holding the soldering pad to the switch. Thus, screw terminals are more reliable by keeping connection repair off the switch. A military grade switch is rugged enough to handle a high speed landing and still function.

2.10 Second Generation Reliability Improvements

The original design had the circuit and radio mounted together on the bottom plate, which caused extra noise on the circuit. This effect was reduced by separating them in two levels with a metal plate. Structure support originally came from metal posts which were replaced by plastic spacers to reduce the instrument weight. There were also battery holders mounted above the circuit that proved difficult to change during field research. Thus, custom-made packs were constructed by spark-welding individual batteries together with thin nickel strips, which also provided leads for soldering. This also improved the current capabilities of battery packs. Views of the original design are shown in Appendix D.

The radio was originally powered on the leads for the rechargeable battery (with the battery removed) instead of the external power jack (Vdc Ext), and the antenna from the VX-2 was used. Both caused the radio to malfunction after a time period ranging from a few days to several weeks. The VX-2 antenna has a standing wave ratio (SWR) of 2.5, as compared to 1.1 for the new antenna, which caused more RF to reflect back to the radio. By changing this configuration to the one described in section 2.6, these problems were eliminated.

CHAPTER 3

Testing and Calibration

3.1 Temperature of Nichrome Wire

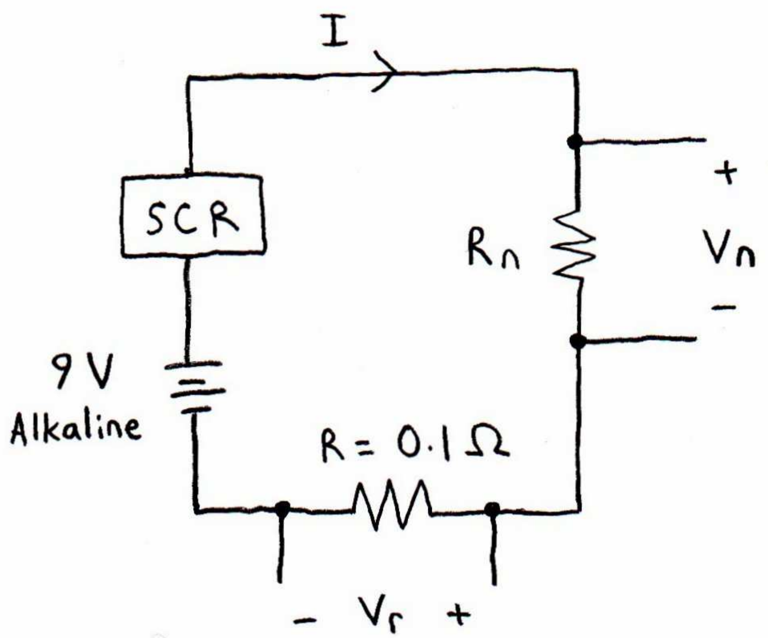

Figure 3.1: Experimental set-up: Used to measure the temperature profile of the nichrome wire during cut-down.

After constructing the instrument, several tests were conducted to determine its effectiveness. The first test was to determine the temperature the nichrome reaches during cut-down activation. The temperature must be higher than the melting point of the monofilament and high enough to melt it in below freezing temperatures. This measurement was accomplished by placing the nichrome in series with a 0.1 Ω resistor and a 9 V battery. A diagram of the experiment is shown in Fig. 3.1.

Equation 3.1 shows the relationship between the resistance and voltage across the nichrome at a given temperature (R_n, V_n), values for the 0.1 Ω resistor (R,V_r), and the current across both (I). Equations 3.2 - 3.6 show the relationships between the power (P) emitted, resistivity (ρ), resistivity at room temperature (ρ_o), temperature (T), temperature coefficient of resistance (α), and resistance of the nichrome wire at room temperature (R_o). The value of α for nichrome is 1.7 x 10^{-4} per ^{o}C (Kuphaldt, 2007). Measured quantities of the side area, length, and resistance of the nichrome wire are A = 5.07 x 10^{-8} m^2, L = 0.035 m, and R_o = 0.76 Ω respectively. The value of 293.15 in the Eq. 3.5 comes from adding 273.15 to convert T from units of ^{o}C to K, and adding the value T_o = 20^{o}C as an offset.

$$I = \frac{Vr}{R} = \frac{V_n}{R_n} \tag{3.1}$$

$$P = IV_n \tag{3.2}$$

$$\rho = \frac{R_n A}{L} \tag{3.3}$$

$$\rho_o = \frac{R_o A}{L} \tag{3.4}$$

$$T(^\circ C) = \frac{1}{\alpha}(\frac{\rho}{\rho_o} - 1) + T_o \tag{3.5}$$

$$T(K) = \frac{1}{\alpha}(\frac{V_n R}{V_r R_o} - 1) + 293.15; \tag{3.6}$$

From these equations, profiles of T, V_n, I, R_n, P, and ρ of the nichrome are produced in Fig. 3.2 - 3.5. The temperature profile shows a maximum value of roughly 2200 K that quickly falls to 1600 K, agreeing with the visual results of a bright orange color temperature during cut-down. This is significantly higher than the melting point of monofilament, which ranges from 500-560 K depending on the type. Thus, this test shows that the instrument has the potential to cut monofilament at low temperatures or high altitudes in the atmosphere. There was a 0.02 Ω uncertainty in the initial resistance of the nichrome, and so red lines representing uncertainty were added in Fig. 3.2.

However, the melting point of nichrome is 1670 K suggesting that the wire is partially melted during the first second of cut-down before cooling to values between 1000 - 1600 K. This agrees with observations of a thinner wire after cut-down. Thus, the wire should be replaced after every flight. Tests with an 18 V supply caused the nichrome to break apart before cutting the monofilament and implies a prolonged temperature above 1670 K.

3.2 Remote Cut-down Software

After testing the cutting ability of the nichrome, the PIC was programmed in C language to decode cut commands using the MicroC compiler and an EasyPIC-4 Chip Development Board from Microelectronika. The code, shown in Appendix G, verifies whether the 3 binary strings sent by the DTMF match a required 3 digit code for cut-down. When the first string is received, the PIC checks whether each of the 4 input pins of Port A are high or low, and stores a 1 or 0 respectively for the variables IN1..4 as a 4-bit binary string. Next, it converts the string into a single digit called DTMF0, which is the

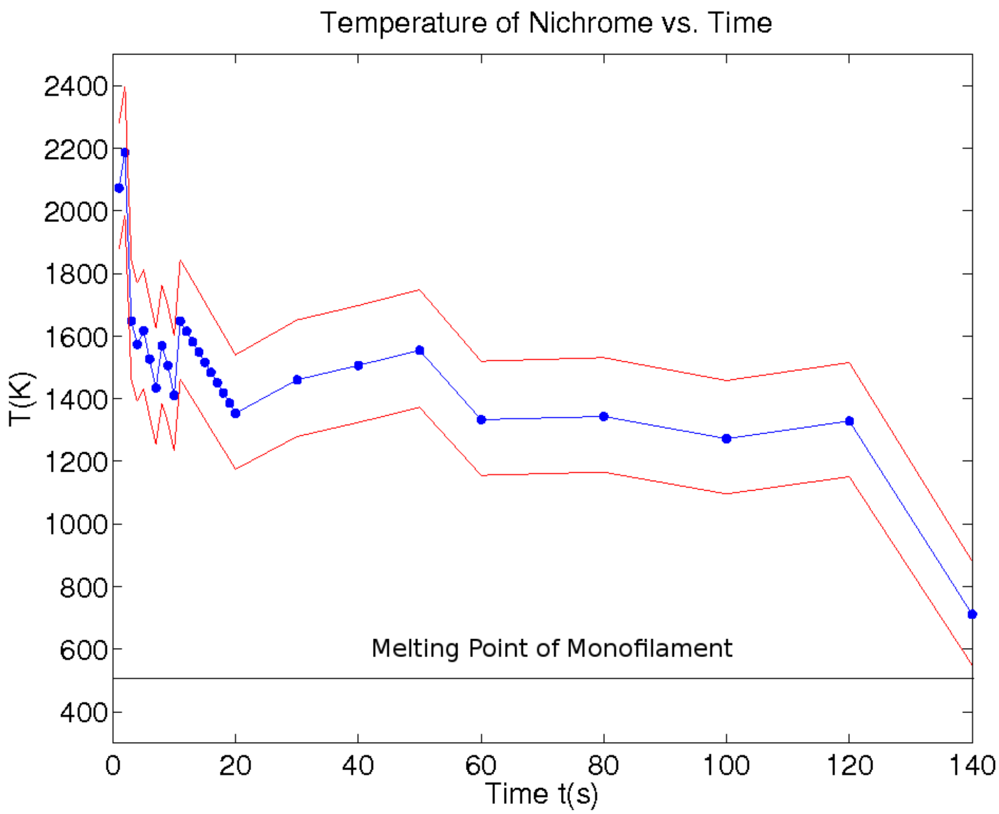

Figure 3.2: Plot of Temperature of Nichrome vs. Time: The blue line is temperature, the red lines are uncertainty in temperature, and the black line is the melting point of monofilament.

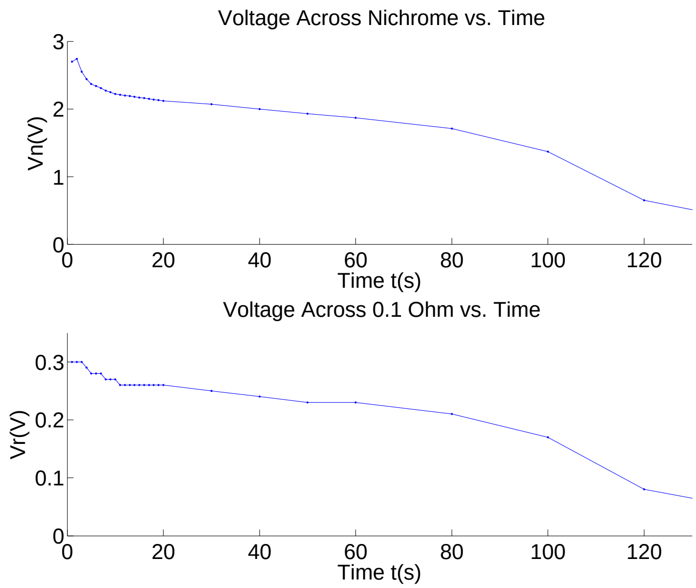

Figure 3.3: Plots of Voltages across Nichrome and 0.1 Ω vs. Time

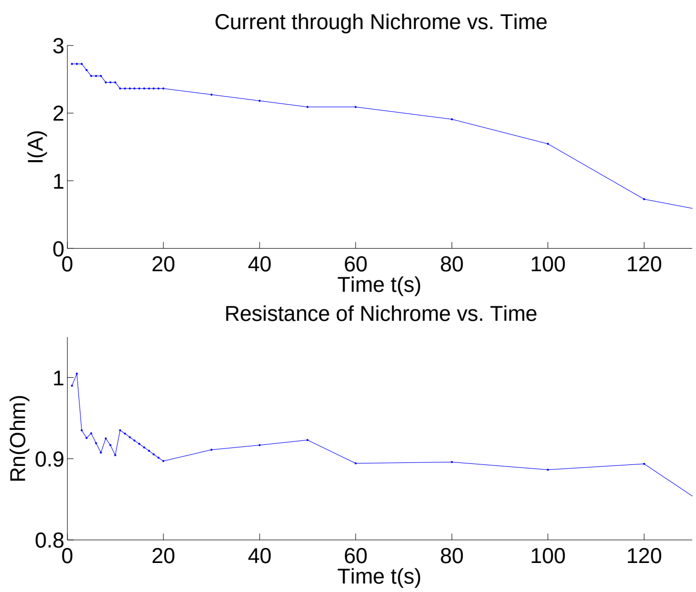

Figure 3.4: Plots of Current and Resistance of Nichrome vs. Time

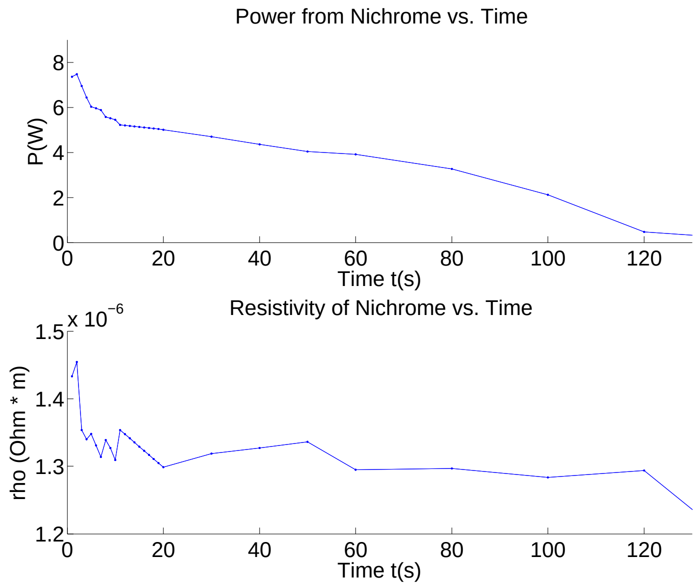

Figure 3.5: Plots of Power and Resistivity of Nichrome Wire vs. Time

first entry of the cut-down code. The code repeats the process for DTMF1 and DTMF2, until a 3 digit code is stored. Then it verifies whether these 3 digits match the ones chosen as the cut-down code. In the case of the example code, the code is 123. If DTMF0..2 match 123, then a TTL high level is sent on output pin 4 (RB3) of Port B, which triggers an SCR for cut-down. Then DTMF0..2 are reset to 0, and the verification process starts over.

Several functions were implemented to improve usability. A 5 second time limit was set to send all 3 digits and have them verified. The variable TimeOut increments by 1 every millisecond, and once TimeOut = 5000, then DTMTF0..2 are reset to 0. In addition, another verification code was put in to act as a transmit mode toggle for the Tinytrak. In the example code, if DTMF0..1 equal A1, then all output pins on PORTB go low for 0.2 seconds. This is enough time to briefly switch transmit modes on the Tinytrak, causing it to transmit its location once. This is valuable to have as the cut-down instrument is approaching the ground and every transmission could give the last known coordinates for finding the instrument.

Although the code eventually proved successful, several problems were encountered in writing it. The line 'CMCON = 0x07' was added to disable comparator mode, which allows pins 1-4 (RA0 - RA3) of Port A to be inputs. When programming the device in MicroC, I determined that RB3 was MCLR or masterclear. This is disabled by selecting the option "MCLRE_OFF" when creating a new project in MicroC, and allows RB3 to be an output. Ports A and B must also have their input/output settings assigned using the appropriate hex entries for TRISA and TRISB respectively. With these additions, the cut-down code verification works and the monofilament is cut on command. Definitions are displayed near the beginning of the code of DTMF output digits corresponding to each button of a touch-tone keypad.

3.3 Timer/Pressure Cut-down

In addition to programming the remote cut-down, the timer circuit must be configured using a combination of resistors and capacitors (referenced from Fig. 2 in Appendix E). The time constant RC is determined by:

$$RC = 0.693 * C3 * (R2 + 2R3) \tag{3.7}$$

For this instrument, the values R2 = 10 kΩ, R3 = 100 kΩ, and C4 = 5 μF were used to produce a time constant of 0.73 seconds. This results in a timed cut-down after 2990 seconds or approximately 50 minutes of operation. The component values were also chosen to satisfy a duty cycle of

0.5 to prevent the LED from using too much power, but to keep it bright long enough for the user to see. Next, the pressure bellows was calibrated using a vacuum chamber and vacuum pump. The assigned pressure level for cut-down is 190 hPa, which corresponds to an altitude of 10.5 km.

3.4 Telemetry

The instrument's telemetry was tested by placing the device on the roof of Workman Center at New Mexico Tech, as shown in Fig. 3.6. By powering the device and waiting for a GPS lock, position data was received by an APRS repeater station on M Mountain. A zoomed-in satellite photo of the instrument's position is shown in Fig. 3.7, from www.openaprs.net. The balloon symbol shows the estimated position while the yellow dot is the actual position.

A range test was conducted on July 5th, 2007 using the VX-2 antenna, to determine a maximum range that the radio can successfully transmit to an APRS station from the ground. The instrument was transported to a location near Socorro Airport until a GPS lock was obtained and transmission was detected on the APRS network. It was then transported southeast and tested approximately every 5 miles with an unobstructed view of the repeater on M Mountain. The results are shown in Appendix H, with GPS time, coordinates, and a description of the location. The time is in coordinated universal time (UTC) and coordinates are in degrees and decimal minutes. Using the last known coordinate and the location of the repeater, a maximum transmission range on the ground was found to be 31.4 miles or 50 km.

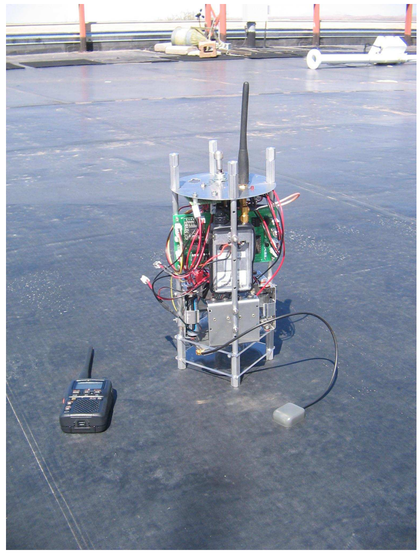

Figure 3.6: Telemetry test: Instrument placed on the roof of Workman Center.

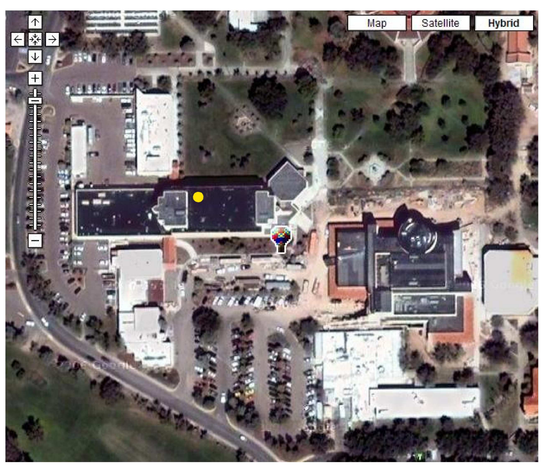

Figure 3.7: Satellite photo provided by APRS network: Estimated instrument location (balloon symbol) and actual location (yellow dot) during telemetry test.

3.5 Antenna Matching

Although the instrument had a reasonable transmission range, it would consistently malfunction after a short period of use. Measurements revealed that the VX-2 had a standing wave ratio (SWR) of 2.5 using it's supplied antenna, and so a new antenna was built. The impedance and SWR of both antennas was tested using an SWR meter shown in Fig. 3.8, with the instrument connected via a coaxial cable and several adapters. Copper wire with 20 gauge was tested at various lengths for an impedance match and SWR near 1. A length of 20.5 +/- 0.1 inches produced an impedance of 50 Ω and an SWR = 1.1.

The wire was then soldered to an SMA adapter[B27] and heat shrink was added as a coating to complete the antenna shown in Fig. 3.9. A close-up view of the adapter is shown in Fig. 3.10. Silicone was added to the base and tip of the heat shrink to prevent water from shorting the wire. This increased the impedance above 50 Ω on some antennas, requiring the wire to be slightly shortened again for an impedance match. Once the antenna was fully constructed, subsequent testing showed that the instrument could transmit to the M Mountain repeater while inside Workman Center.

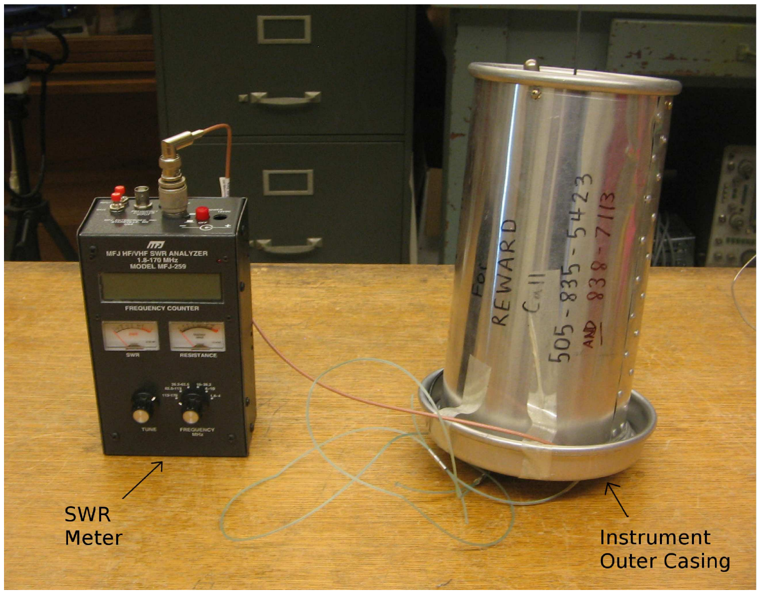

Figure 3.8: Test set-up: Used to determine the new antenna length.

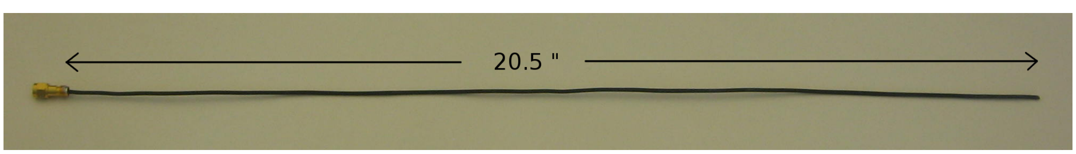

Figure 3.9: Custom-built antenna with an SWR = 1.1.

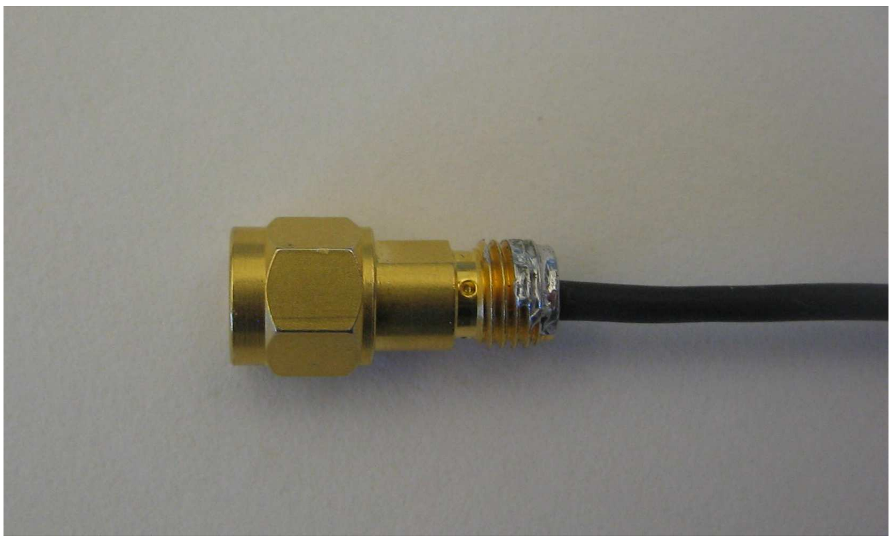

Figure 3.10: Adapter on antenna that attaches to bottom of instrument.

CHAPTER 4

Initial Flight Results

4.1 Test Flight

Before the addition of a new antenna, the first generation instrument was flown in a test flight on July 30th, 2007. The instrument was connected to a 1200 g latex balloon, and had nichrome installed on both the timer/pressure and remote cut-down circuits. The balloon began ascent at 11:25 AM from the balloon hangar at Langmuir Laboratory, reaching a maximum altitude of 9.2 km above sea level. Command cut-down was activated near this time, and further altitude recordings showed that the instrument was descending. It was tracked to a distance of 12.1 km and to an altitude of 2.1 km which corresponded to ground level.

Although, the instrument was successfully tracked to the ground, the instrument stopped transmitting within 10 hours. It began working again for several hours after a power cycle. The pressure cut-down activated before the cut command as demonstrated by oxidation of the nichrome wires as well as the length of monofilament present inside the instrument. Plots of altitude and distance vs. time are shown in Fig. 4.1.

A second test flight was flown on April 14th, 2008. The instrument was fitted with the new antenna and with the pressure/timer cut-downs disabled. The balloon reached a maximum altitude of 18 km above sea level, upon

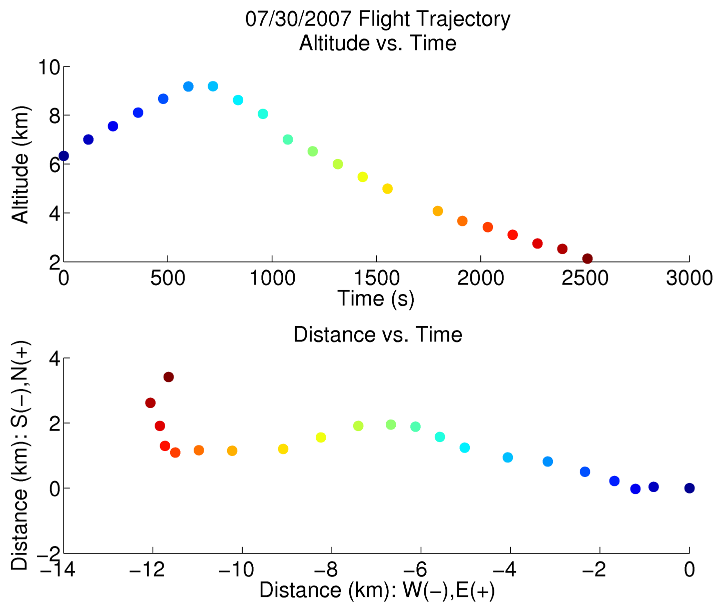

Figure 4.1: Plots of altitude and distance vs. time: Test flight 1.

which a command cut-down was activated. Further altitude recordings showed that the instrument was descending, indicating the cut command worked. It was tracked to a distance of 60 km and to an altitude 800 feet above ground level, after which no transmissions were received. After two searches, the instrument was not recovered. Plots of altitude and distance vs. time are shown in Fig. 4.2.

4.2 E-sonde Instrument Flights

After the success of the first test flight, the instrument was used in three E-sonde flights, each containing a different cut-down instrument fitted with the original antenna. The first flight was on August 9th, 2007, and began at 3:15 PM. The balloon was tracked to a maximum altitude of 13.3 km, upon which the pressure sensor activated cut-down. A cut command was not issued

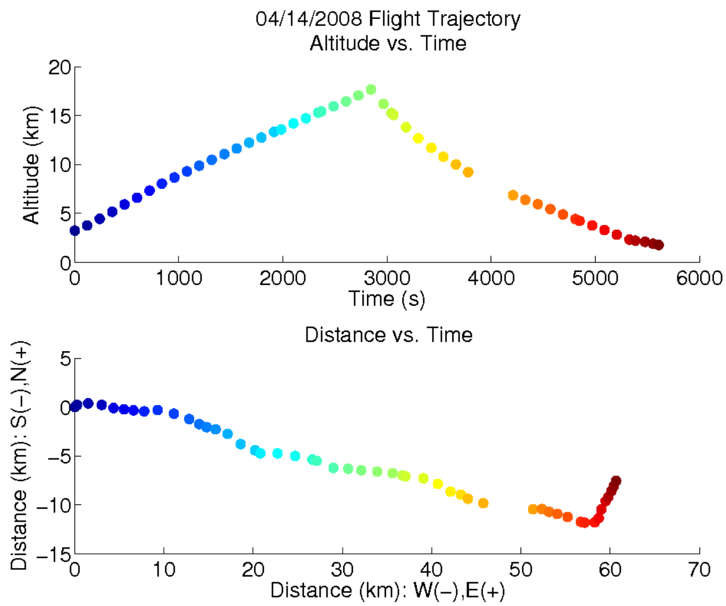

Figure 4.2: Plots of altitude and distance vs. time: Test flight 2.

first because the balloon was moving over mountainous terrain. However, a cut command was issued later on as a test.

The instrument was tracked using APRS to a distance of 15.9 km and altitude of 3.5 km, with plots shown in Fig. 4.3. The E-sonde was tracked with a different antenna in the cupola at Langmuir to a final landing site. Upon retrieval, the cut-down instrument was found to be transmitting at a short range 24 hours since being turned on. In addition to having a high SWR, the antenna was slightly bent which could possibly explain the poor transmission range. The cut command was found to be successful after inspection of both nichrome wires.

The second flight was on August 24th, 2007, and began at 3:55 PM. The balloon was tracked to a maximum altitude of 13.3 km as shown in Fig.

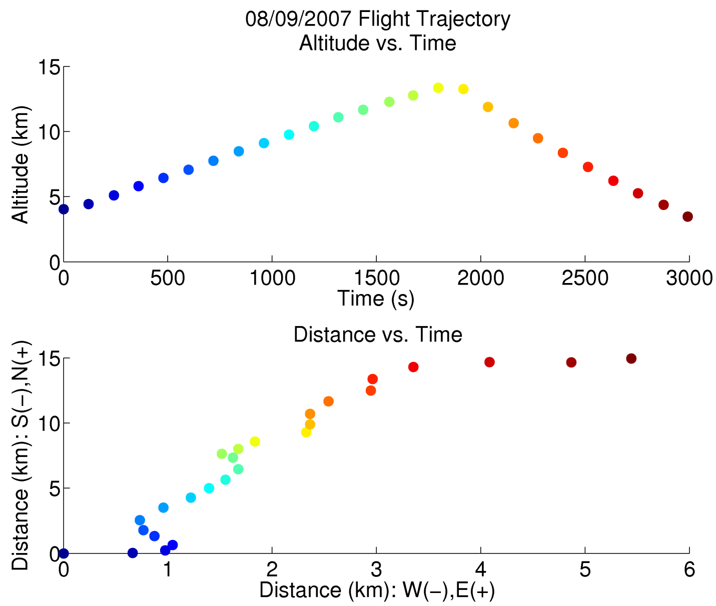

Figure 4.3: Plots of altitude and distance vs. time: E-sonde flight 1.

4.4, upon which a cut command was issued. The last packet was received at a distance of 32.6 km and altitude of 2.1 km, and the E-sonde was tracked with it's telemetry to the landing site. In this case, the APRS telemetry did not provide enough data to retrieve the instruments, and the E-sonde telemetry was needed. Retrieval of the instruments showed that the instrument was transmitting at short range 24 hours since being turned on. It was determined that the pressure sensor again cut before the cut command was issued. However, both types of cut-down worked. The antenna was bent again from the impact of landing.

The third flight was on August 30th, 2007. Although no flight log was recorded for the cut-down instrument, several long intervals were observed with no transmissions. A cut command was issued slightly after the instrument began descent, indicating that the pressure sensor cut first. While descending,

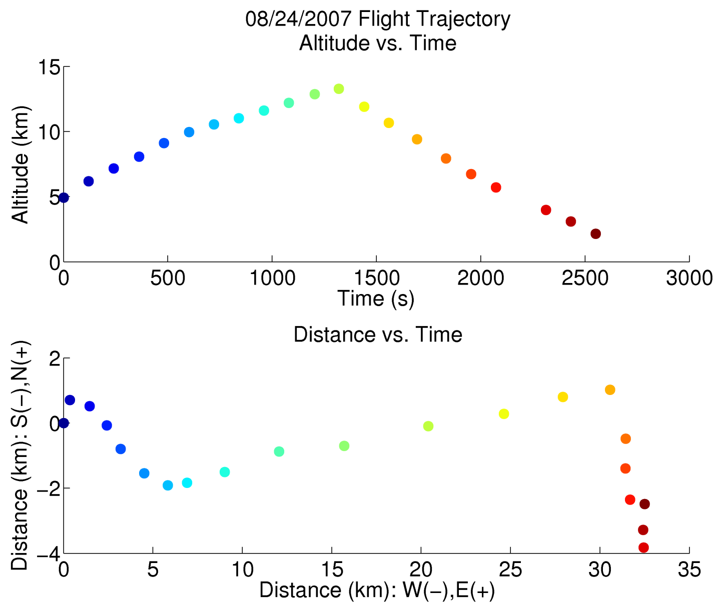

Figure 4.4: Plots of altitude and distance vs. time: E-sonde flight 2.

the parachute became tangled and the controller landed at free fall. Upon retrieval, it was transmitting at short range. The cut-down instrument suffered mild damage to the case, as well as a bent antenna.

CHAPTER 5

Conclusion and Future Plans of the Instrument

From these flights, its clear that this instrument has the ability to detach scientific payloads from helium balloons remotely or with a timer/pressure sensor on board. The temperature of the nichrome wire on the cut-down circuit reaches a value several times higher than the melting point of monofilament, demonstrating an ability to detach payloads at very high altitudes. The instrument also performs successfully as a tracking instrument, and has been tested on the ground and in the air to transmit GPS coordinates of its location to APRS repeaters up to a distance of 60 km. The APRS network displays the instrument's location on a map with an overlay of terrain and weather radar. Multiple instruments can function simultaneously if the transmission rate of each has a small offset relative to the others. If a new antenna is designed that can survive a landing, and the transmit toggle is used frequently near the time of landing, this system on its own provides enough data for reliable recovery of a payload.

The success of the cut-down instrument suggests that it can be used to retrieve multiple E-sondes in a single flight. However, with small modifications, the instrument can be used for other types of experiments in conjunction with a scientific payload. The RC constant on the timer circuit can be increased, and the pressure bellows removed, to assist in long duration, high-altitude balloon measurements of sprites. Two instruments can be used at once in a constant altitude balloon flight to assist with simultaneous measurements of X-rays and E-fields in a thunderstorm to test the theory of runaway breakdown. The addition of a landing site prediction algorithm to the ground station will aid in the timing of remote cut-down. In future designs, the instrument will also act as an airborne controller for other payloads attached to the balloon by transmitting instrument data, providing a time reference, and allowing payloads to be commanded from ground.

CHAPTER 6

Introduction to the Correlation Study

6.1 Goals of the Study

In addition to developing an instrument, I sought to find a correlation between number of lightning flashes in 24 hours (N) and other weather variables derived from atmospheric soundings. The goal was to find a way to forecast afternoon thunderstorms using the AM sounding from a National Weather Service (NWS) station. The ability to better predict storms, even a few hours in advance, would, at minimum, help atmospheric researchers conduct more efficient field studies. Correlations were sought primarily between N, convective available potential energy (CAPE), mixing ratio of water vapor to air (MR), dry-bulb temperature (T), and wind speed (WS), on the ground and aloft. We did not expect a correlation for these latter two variables, and for this reason, they were chosen as statistical controls. My assumption at the outset was that CAPE would correlate well with the presence of storms, due to the well known relationship between CAPE and the maximum updraft speed, w, in a storm (Williams and Renno, 1993):

$$w = \sqrt{2 * CAPE} \tag{6.1}$$

The non-inductive charging model of cloud electrification assigns importance to updrafts, because they cause graupel and ice particles to collide and exchange charge. Takahashi (1978) and Jayaratne et al. (1983) showed that a steady stream of ice crystals with no liquid later impinging on riming ice in the presence of tiny water droplets led to the development of opposite polarities by the different species of hydrometeors. Updrafts separate the different species by differential drag based on their differing sizes. Williams (1989) states that updraft winds would keep ice crystals and supercooled water droplets aloft for a longer amount of time to form graupel. Stronger updrafts would also cause the graupel particles to fall at a slower rate, thus allowing more time for collisions with ice particles to produce charge transfer. This effect could be responsible for building and maintaining the large electric field that forms in a cloud during a thunderstorm.

6.2 A Comparison to Prior Correlation Studies

Although CAPE theoretically shows promise for lightning prediction, past studies display mixed results. Livingston et al. (1996) found a correlation coefficient of 0.48 between CAPE and N in a study done for the 1996 Summer Olympic games in Georgia. Qie et al. (2003) found a nonlinear relationship between both variables in the central Tibetan Plateau. In contrast, Molinie and Pontikis (1995) found no correlation in the French Guyana coast. These results suggest that the correlation varies from region to region. This is probably because CAPE is related to the maximum updraft speed and is only a rough estimate of atmospheric instability (Doswell et al., 1994; Lucas, 1994). The efficiency with which CAPE is converted to vertical kinetic energy varies as well for locations with different terrain and atmospheric water content.

The significance of CAPE in comparison to water content for flash counts has come into question. If the E-field in a thunderstorm indeed depended on ice/graupel collisions, then the strength and duration of the field would certainly require some moisture in the air to form ice, as well as below freezing temperatures in clouds needed to form graupel. Jayaratne has also shown that the charge transfer per collision has a dependence on the water content of the ice particles. From data collected by the Tropical Rainfall Measuring Mission (TRMM) satellite over a span of 11 years, Peterson et al. (2005) showed that a correlation exists throughout the world between the ice water content of the atmosphere and lightning. While there have been CAPE studies, we found no published work on the correlation between MR and N. However, it is rumored that Charles B. Moore, working at Langmuir Laboratory in the 1970's, observed that thunderstorms occurred at the lab when the relative humidity was high in the morning (Richard Sonnenfeld, New Mexico Tech, rsonnenf@nmt.edu, private communication).

CHAPTER 7

Research Methods for Correlation Study

7.1 Los Alamos Sferic Array

To determine the importance of CAPE, data was analyzed from the Los Alamos Sferic Array (LASA) containing total lightning flash counts from the summer months of 2005 and 2006. The array consists of a series of stations that each contain a sensor designed to detect the transient E-field change produced by a lightning discharge (Shao et al., 2006). They each consist of a charge amplification circuit connected to a sensing plate, with a stainless steel dome suspended above to prevent raindrops from hitting the plate and producing extraneous signals (Smith et al., 2002). The stations have a GPS receiver connected to a computer that provides UTC lightning strike time tagging with a maximum error of 2 μs (Shao et al., 2006). In April 2004, eight upgraded stations were deployed in the Northern-Central Florida Array (Shao et al., 2006). Other stations have been implemented in Los Alamos, NM; Greeley, CO; Lincoln, NE; Garden City, KA; Norman, OK; and Lubbock, TX; as part of the Great Plains Array (Xuan Min Shao, Los Alamos National Laboratory, xshao@lanl.gov, 2007, private communication).

Lightning data in this study were obtained from LASA to find the total lightning flash count N within 100 km radii of the following NWS stations: Albuquerque, NM; El Paso, TX; Flagstaff, AZ; Tucson, AZ; Denver,

Month	Days (2005)	Days (2006)
May	24 - 31	N/A
June	1 - 16, 18 - 30	1 - 30
July	1 - 31	1 - 31
August	1 - 7, 25 - 30	1 - 31
September	20 - 23	N/A
Total	85	92

Table 7.1: Lightning Data Range

CO; Norman, OK; Peachtree, GA; and Tampa Bay, FL. These locations are significant because of their close vicinity to LASA stations, as shown in Fig. 7.1. The detection accuracy of LASA declines with increasing distance away from a station. LASA location error is within 4 km near the center of the Great Plains array, and gradually increases with distance as shown in Fig. 7.2 (Shao, 2007, personal communication). At locations within the Florida array, the detection error was less than 500 m as shown in Fig. 7.3 (Shao et al., 2006). These weather stations are also located in areas with large amounts of CG lightning (Orville et al., 2001). The accuracy of LASA data was determined by comparing its results to those of the National Lightning Detection Network (NLDN), which detects the same flashes as the Continental United States (CONUS) satellite. CONUS has a detection efficiency of 90 % for CG strokes in the continental U.S. (Shao et al., 2006). The days present in the collection are shown in Table 7.1.

7.2 Upper Air Balloon Soundings

LASA data were compared with meteorological parameters from upper air balloon soundings. These are sets of data collected by a radiosonde that

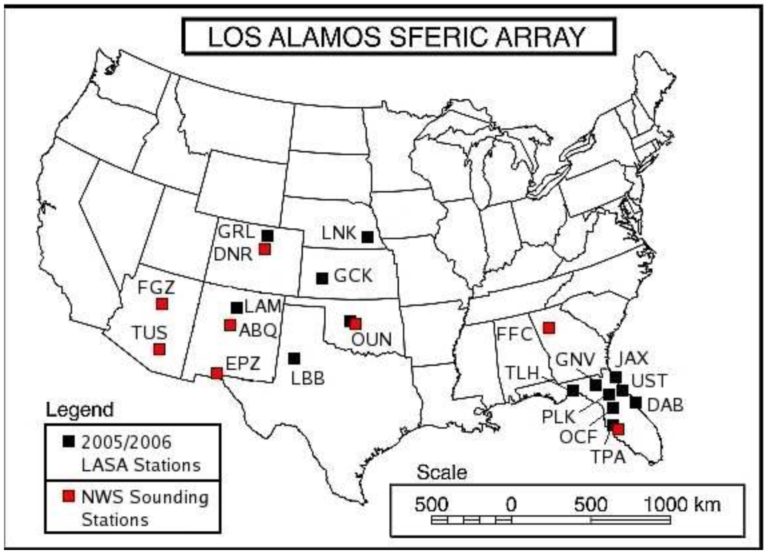

Figure 7.1: LASA and NWS Upper Air Sounding Stations (Modified from Smith et al., 2002): NWS stations were chosen that lie near the LASA array.

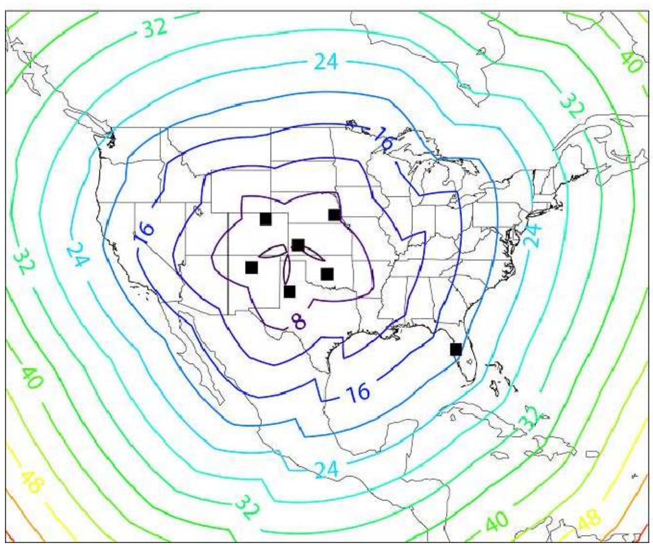

Figure 7.2: Location Error of the Great Plains Array (Shao, 2007, personal communication): Contours represent error in km.

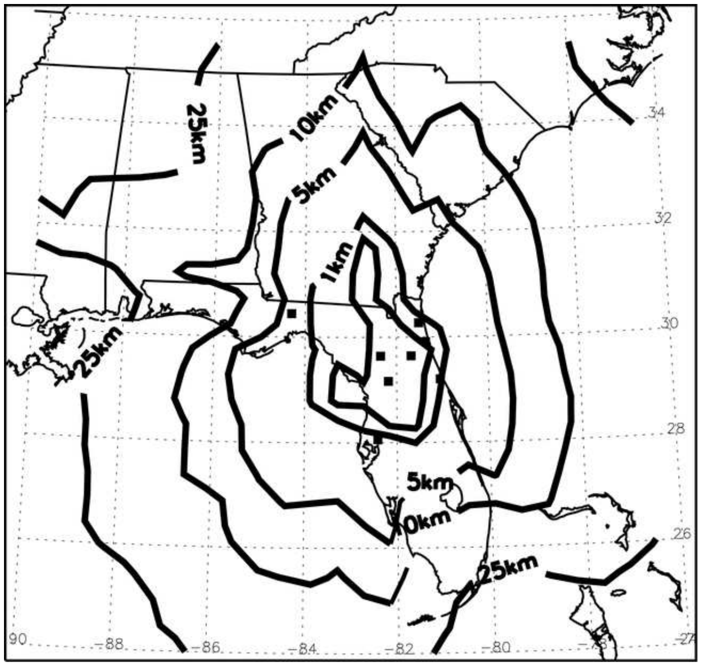

Figure 7.3: Location Error of the Florida Array (Shao et al., 2006)

travels upward through the atmosphere. The launch protocols for soundings we used are listed in the Federal Meteorological Handbook N. 3 (FCM-H3-1997). The sonde is part of an airborne train consisting of a latex balloon filled with either hydrogen or helium, a parachute, and the instrument at the bottom. Sondes typically drift up to 300 km during flight (FCM-H3-1997). Since our goal was correlating sounding and LASA data on the same parcel, we chose 100 km as a nominal radius around the sounding launch site in which to search for lightning in order to correlate parameters with local air masses.

The data collected during a sounding consists of air temperature, relative humidity, wind speed and direction, and atmospheric pressure, at different heights in the atmosphere. From this data several other variables can be cal-

Station	Sonde	Ground
Albuquerque, NM	Sippican B2	ART (Automated Radio Theodolite)
El Paso, TX	Vaisala RS80-57H	ART
Flagstaff, AZ	Vaisala RS80-57H	ART
Tucson, AZ	Vaisala RS80-57H	ART
Denver, CO	Vaisala RS80-57H	ART
Pittsburgh, PA	Sippican B2	ART
Norman, OK	Vaisala RS80-57H	ART
Tampa Bay, FL	Vaisala RS80-57H	ART

Table 7.2: Ground and Airborne Instruments at Sounding Stations

culated, including MR and CAPE, using algorithms shown in Appendix G. Data accuracy is within 0.5^o C for air temperature, 5 % for relative humidity, 1.5 m/s for wind speed, 2.0 hPa for pressure greater than 300 hPa, and 1.5 hPa for pressure less than 300 hPa (FCM-H3-1997).

The ground and airborne instruments used for soundings at each station are shown in Table 7.2 [1]. Sounding data were obtained from the University of Wyoming's Atmospheric Science Department [2] and the Integrated Global Radiosonde Archive (IGRA) [3]. Values of MR, CAPE, T, and WS at both ground level and 500 hPa were collected from the AM (1200 UTC) and PM (0000 UTC) soundings. The type of CAPE listed at UW's website is mean mixed-layer CAPE from the lowest 500 m. Thus, when summing CAPE, the first term in the summation is found using the average values in the lowest 500 m for each parameter in the calculation.

Both AM and PM soundings were used because they were both avail-

[1] William Blackmore, NOAA/NWS, william.blackmore@noaa.gov, private communication
[2] http://weather.uwyo.edu/upperair/sounding.html
[3] http://www.ncdc.noaa.gov/oa/climate/igra/index.php

able and because of the large amounts of lightning present throughout the entire day, as shown in Fig. 7.4 from the LASA data. Comparisons between flash count and meteorological parameters at 500 hPA are useful because moisture is lifted vertically by convection to form thunderstorm clouds. At 500 hPa the temperature in most soundings is near -10^o C, the charge reversal temperature for ice/rimed graupel collisions (Takahashi, 1978). The height corresponding to 500 hPa is roughly 5.5 km which, according to Stolzenburg et al. (1998) and Krehbiel (1986), is near the region where charges separate in a New Mexico thunderstorm. Electric field soundings conducted by Marshall and Rust (1991) also consistently show strong positive/negative fields closely above/below this altitude for storms in New Mexico and Oklahoma.

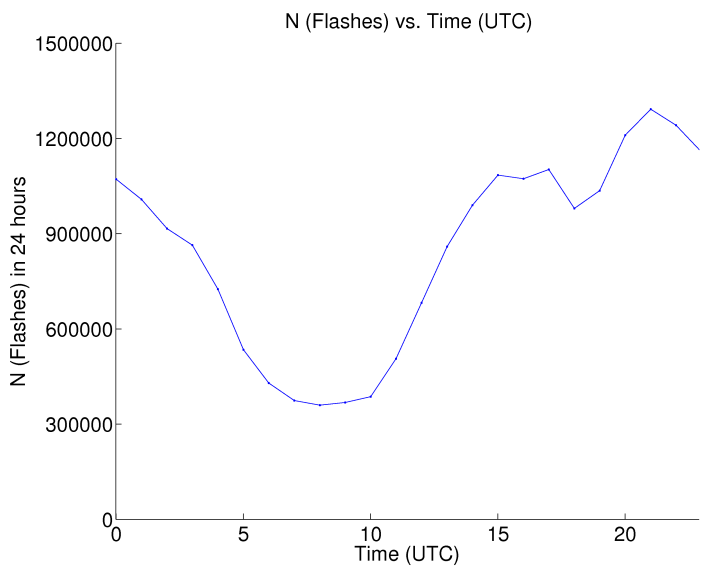

Figure 7.4: Plot of N vs. Time of Day: Illustrates the similar amounts of lightning during AM and PM hours.

7.3 Comparing Lightning Data with Sounding Data

After organizing the sounding data into a usable format, log-log plots of each parameter vs. N were generated. The reason for this type of plot is due to the large numerical variation of N in comparison to the other parameters, and to allow linear correlation to be used. To quantify the correlation, r coefficients were calculated for each comparison using the following equation (Taylor, 1996):

$$r = \frac{\sum (x_i - \overline{x})(y_i - \overline{y})}{\sqrt{\sum (x_i - \overline{x})^2 \sum (y_i - \overline{y})^2}} \tag{7.1}$$

The closer r approaches 1 or -1, the higher the correlation (either positive or negative). Plots and r values were generated for each variable, sounding, and pressure level. Plots were also made for different ranges around each station, with distances of 50 to 500 km, to see how the correlations change with increasing distance. After log-log plots were analyzed, direct plots of lightning counts and weather variables over time, as well as probability charts for lightning, were analyzed to detect trends in the data.

CHAPTER 8

Results

8.1 Mixing Ratio of Water to Air

The mixing ratio at ground level showed the strongest correlation with lightning for stations located in the Southwest. A log-log plot of MR vs. N for all stations is shown in Fig. 8.1. The distribution shows that the maximum number of flashes within a 100 km radius of any station during the summer months can be estimated using the mixing ratio. A log-log plot of MR vs. N for Albuquerque, NM, is shown in Fig. 8.2. The points approximately fall on lines with positive slopes. A plot of both ln(N) and MR at Ground Level vs. Day of Study for Albuquerque, NM is shown in Fig. 8.3. A linear increase in mixing ratio usually corresponds with an exponential increase in lightning, and for several data points MR and ln(N) are nearly equal.

A plot of the probability of at least 1 flash vs. MR is shown in Fig. 8.4 for stations in the Southwest. The probability has a plateau between 0.9 - 1 for each station as MR approaches 10 g/kg. In the case of Tucson, there is no plateau and the probability is 1 for all MR greater than 16 g/kg. A probability plot of at least 1 flash within 25 km of Langmuir vs. MR at 5 AM is shown in Fig. 8.5. The 5 AM plot was most useful for storm prediction because for other times all values of MR had similar probabilities. A value of MR between 7 and 8 g/kg at 5 AM corresponded to a maximum probability of 0.85 for a

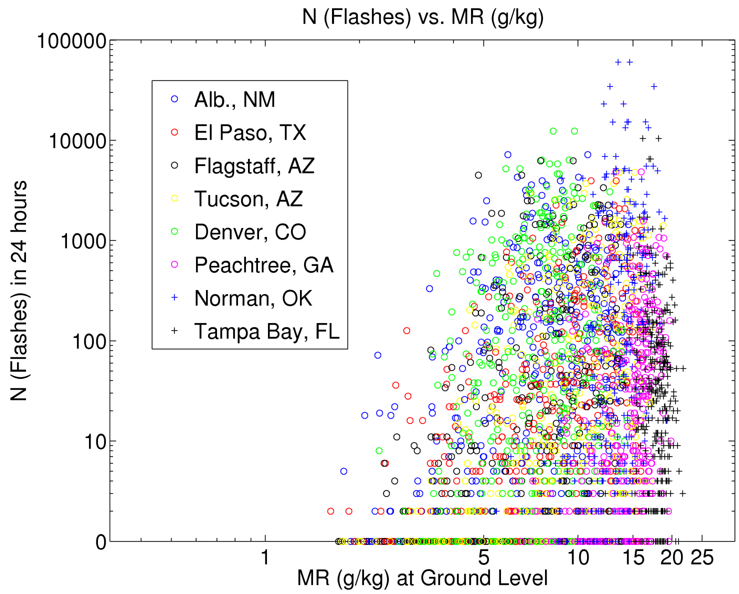

Figure 8.1: Plot of N vs. MR for all stations: Illustrates that an upper bound exists for N at any stations for a given value of MR

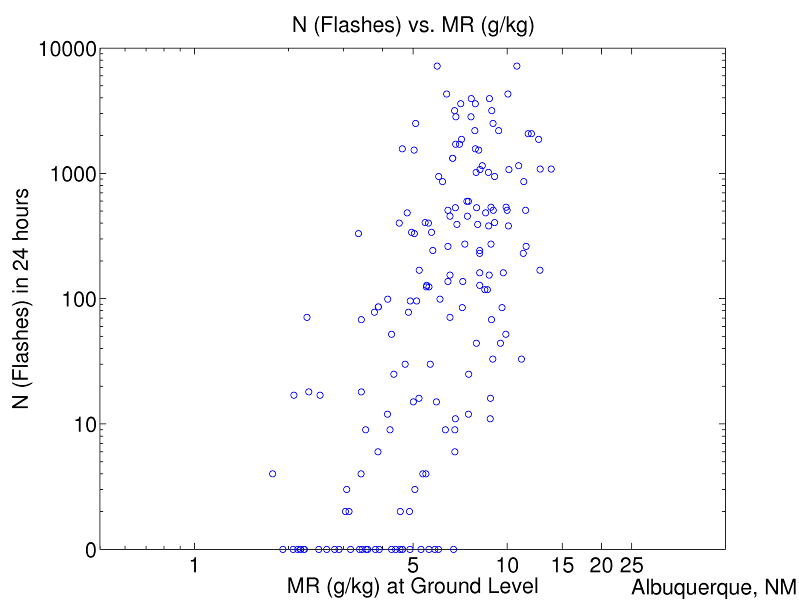

Figure 8.2: Plot of N vs. MR: A linear increase in MR corresponds to an exponential increase in N for stations in the Southwest.

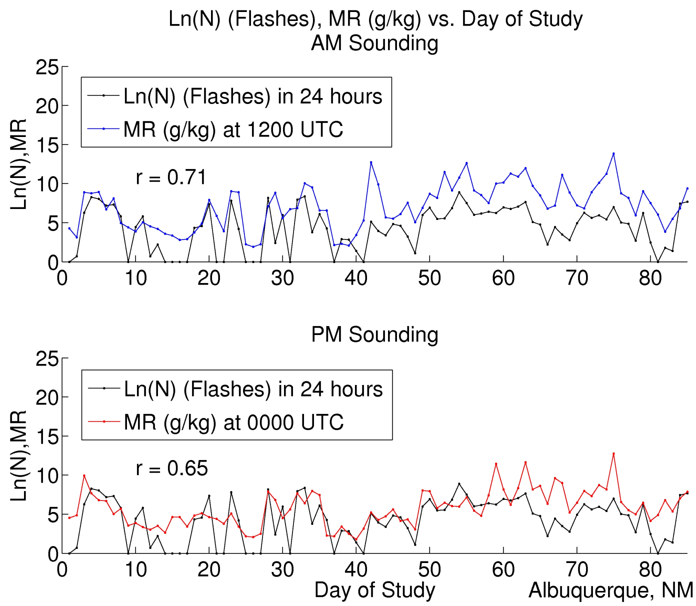

Figure 8.3: Plot of ln(N), MR vs. Day of Study: The relationship MR $\approx$ ln(N) occurs for the Southwest.

lightning flash to occur that day.

The average r value for the Southwest was 0.7 for both the AM and PM soundings as shown in Table 8.1. The MR measured at 500 hPa generally correlated less well than the MR obtained at ground level. MR values from the AM sounding that always occurred with lightning ($N > 0$) were 7 g/kg for stations in New Mexico and Texas, and 8 g/kg in Arizona. For the PM sounding in Colorado, the corresponding MR value was only 4 g/kg. Table 8.2 shows that the r values at Langmuir are highest in the early morning and decrease throughout the day, consistent with the AM/PM contrast at other stations.

To gain greater confidence that the apparent correlation between MR and N was causal and related to properties of the air-mass measured by the

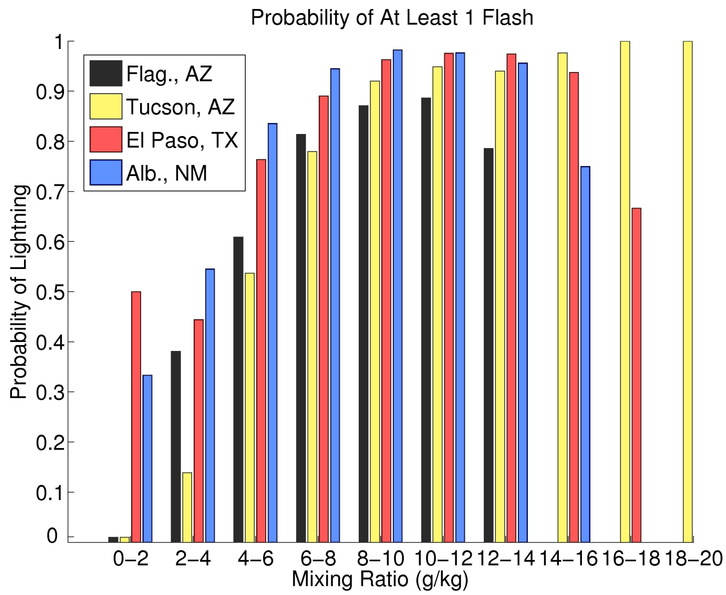

Figure 8.4: Plot of P(N>0) Within 100 km of NWS Station vs. Mixing Ratio for Southwest stations

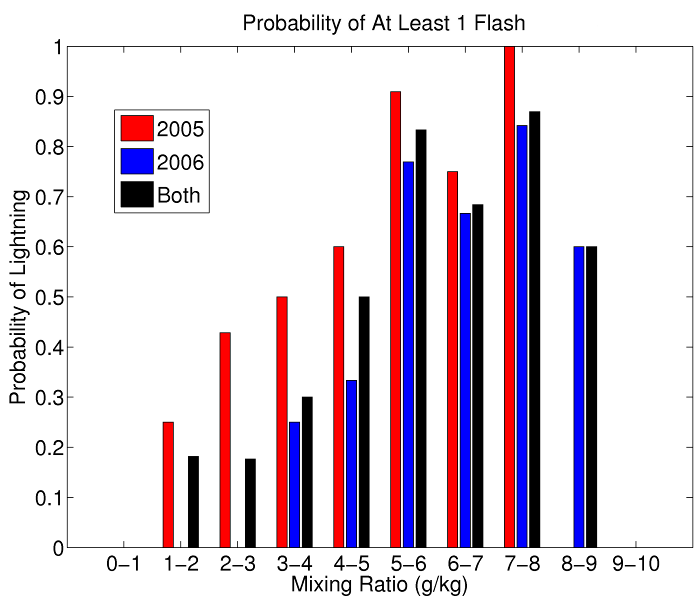

Figure 8.5: Plot of P(N>0) Within 25 km of Langmuir vs. Mixing Ratio

Station	AM/Ground	AM/500 hPa	PM/Ground	PM/500 hPA
Albuquerque, NM	0.71	0.49	0.65	0.22
El Paso, TX	0.70	0.48	0.68	0.49
Flagstaff, AZ	0.75	0.63	0.76	0.64
Tuscon, AZ	0.74	0.60	0.79	0.57
Denver, CO	0.27	0.49	0.52	0.24
Norman, OK	0.10	0.29	0.28	0.17
Peachtree, GA	0.19	0.27	0.14	0.40
Tampa, FL	-0.15	0.06	-0.08	0.09

Table 8.1: r Correlation Coefficients for MR

sounding, the radius was expanded about the sounding location in which N was counted. Table 8.3 shows the results. For 3 of the 4 stations in the Southwest, the correlation between MR and N is constant until flashes that occurred 300-500 km distant from the sounding site are included. At this distance, the correlation falls off substantially.

The range of distances over which MR and N correlate best is consistent with the range over which mixing is likely to occur in a day, as well as published guidelines suggesting that balloon soundings characterize air masses within a distance of 300 km from the sounding site (FCM-H3-1997). If MR and N had no causal relationship, we would expect that N would not depend on the distance away from the location of the MR measurement.

8.2 CAPE

CAPE has significantly less correlation with N than does MR. A log-log plot of CAPE vs. N for all stations is shown in Fig. 8.6. The scattered points show no apparent correlation. It is instructive to compare this plot with that of Fig. 8.1. Though 8.1 data has significant scatter, each MR value

Time	Mixing Ratio	Wind Speed	Temperature
5 AM	0.63	-0.51	-0.08
6 AM	0.63	-0.25	-0.07
7 AM	0.64	-0.53	-0.06
8 AM	0.64	-0.42	-0.03
9 AM	0.42	-0.22	0.11
10 AM	0.44	-0.29	0.08
11 AM	0.45	-0.22	0.07
12 PM	0.44	-0.14	0.07
1 PM	0.44	-0.24	0.08
5 PM	0.07	-0.22	-0.11

Table 8.2: r Correlation Coefficients for Langmuir

Station	75 km	100 km	150 km	200 km	300 km	500 km
Albuquerque, NM	0.67	0.71	0.67	0.67	0.68	0.42
El Paso, TX	0.68	0.70	0.71	0.73	0.64	0.47
Flagstaff, AZ	0.75	0.75	0.74	0.75	0.74	0.73
Tuscon, AZ	0.74	0.74	0.74	0.71	0.69	0.63

Table 8.3: r Correlation Coefficients for Ground Level MR at Varying Distances from Station

clearly correlates to a maximum N value. Figures 8.1 and 8.6 suggest that water content plays a stronger role than convection in determining flash rates during the summer months. As was done for MR, R values for N vs. CAPE were calculated at different ranges from the sounding station. Table 8.5 shows the r values are relatively constant with increasing distance and only fall off when the distance approaches 300 km.

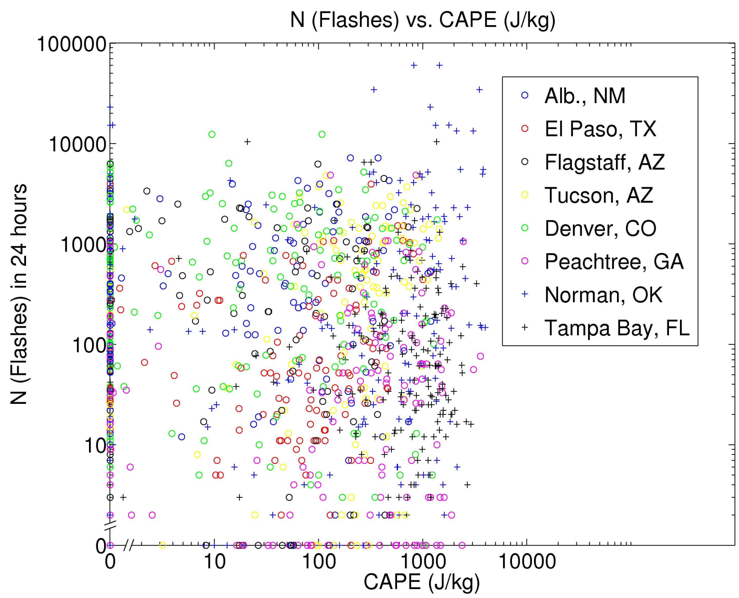

Figure 8.6: Log-Log Plot of CAPE vs. N for All Stations

8.3 Air Temperature and Wind Speed

Temperature and wind speed were selected as 'control' variables. I assumed they would not correlate well with N. Tables 8.6 and 8.7 confirm our opinion that neither variable is a good predictor of lighting. Surprisingly, there were weak negative correlations for WS aloft in the Southwest, as well as T aloft in Oklahoma. A trend that did appear at all stations was a negative T

Station	AM CAPE	PM CAPE
Albuquerque, NM	0.49	0.45
El Paso, TX	0.45	0.50
Flagstaff, AZ	0.51	0.29
Tucson, AZ	0.72	0.71
Denver, CO	0.18	0.04
Norman, OK	0.17	0.15
Peachtree, GA	0.13	0.08
Tampa, FL	-0.11	0.06

Table 8.4: r Correlation Coefficients for CAPE

Station	75 km	100 km	150 km	200 km	300 km	500 km
Albuquerque, NM	0.47	0.49	0.45	0.44	0.40	0.23
El Paso, TX	0.41	0.45	0.44	0.45	0.38	0.32
Flagstaff, AZ	0.52	0.51	0.50	0.49	0.46	0.41
Tuscon, AZ	0.72	0.72	0.69	0.67	0.64	0.57

Table 8.5: r Correlation Coefficients for AM CAPE at Varying Distances from Station

correlation for the PM sounding. However, these correlations have no predictive value.

8.4 Discussion

The Southwestern U.S. was significantly dryer than the rest of the country during the summer months of 2005 and 2006, as shown Table 8.8, suggesting that MR could be a limiting factor for storm formation. This table also suggests that MR is probably not a limiting factor for storm formation in Oklahoma and Florida. Total precipitable water (TPW) was also analyzed and found to correlate roughly the same with flash counts as MR at all stations. It was also determined that the average values of TPW at each station followed the same order as the above table.

Station	AM/Ground	AM/500 hPa	PM/Ground	PM/500 hPA
Albuquerque, NM	0.26	0.03	-0.31	0.22
El Paso, TX	0.17	0.07	-0.37	0.20
Flagstaff, AZ	0.63	-0.11	-0.54	0.01
Tuscon, AZ	0.35	0.08	-0.29	0.23
Denver, CO	0.06	-0.21	-0.41	-0.14
Norman, OK	-0.04	-0.45	-0.28	-0.47
Peachtree, GA	0.16	-0.05	-0.05	-0.11
Tampa, FL	-0.13	-0.27	-0.43	-0.15

Table 8.6: r Correlation Coefficients for T

Station	AM/Ground	AM/500 hPa	PM/Ground	PM/500 hPA
Albuquerque, NM	0.33	-0.20	0.13	-0.18
El Paso, TX	0.06	-0.36	-0.13	-0.23
Flagstaff, AZ	0.36	-0.31	-0.36	-0.27
Tuscon, AZ	0.24	-0.29	-0.18	-0.36
Denver, CO	-0.17	0.01	0.20	-0.05
Norman, OK	0.24	0.14	0.05	0.17
Peachtree, GA	0.06	-0.03	0.03	-0.14
Tampa, FL	0.00	0.03	-0.11	0.10

Table 8.7: r Correlation Coefficients for WS

Station	Average Mixing Ratio (g/kg)
Albuquerque, NM	6.45
El Paso, TX	6.75
Flagstaff, AZ	6.05
Tucson, AZ	7.90
Denver, CO	7.20
Norman, OK	13.50
Peachtree, GA	14.74
Tampa Bay, FL	17.75

Table 8.8: The values in NM, TX, and AZ are significantly lower than other areas.

The fact that MR in the morning correlates the most with N at Langmuir Laboratory suggests that moisture near the ground plays a role with charging mechanisms later in the day. The daily convective cycle begins at sunrise when solar radiation reaches the atmosphere, heating the earth's surface. This causes warmer, moist air to rise above the lifted condensation level (LCL), thereby releasing latent heat through phase changes into liquid water and ice. At this point, moisture has been lifted to heights great enough for mixed-phase charging mechanisms to take place later in the day. Thus, moisture from the ground could eventually have an effect on the magnitude of electric fields aloft.

Because single-cell storms in the Southwest typically last less than two hours, as compared to the many hours or days of frontal storms characteristic of the Midwest, MR measured at an NWS station would correlate with lightning in air masses that remain within 100, or even 300 km, of the measurement after 24 hours have passed. This might not be the case in other regions such as Oklahoma.

Although horizontal wind speeds have little role in electric field generation, Raymond and Wilkening (1985) suggest that they decrease in the vicinity of clouds that produce a thunderstorm in the Southwest. Since most storms in this region form over mountaintops, strong horizontal winds would blow the vertical cloud development off the mountain and prevent the storm from forming. This could explain the negative correlation for wind speed and lightning at 500 hPa at stations in the Southwest, as well as the ground measurements at Langmuir Lab.

CHAPTER 9

Conclusion and Future Plans of the Correlation Study

From the results, it is clear that MR has a strong correlation with N in the Southwestern U.S. This is also one of the driest areas in the country, suggesting that water content is a limiting factor for storm formation. MR can predict afternoon thunderstorms based on the value from a balloon sounding or simply a measurement on the ground. It can also be used to estimate the maximum number of flashes in 24 hours within a 100 km radius of any weather station in the U.S. In general, the mixing ratio has a significantly stronger correlation with flash counts than does CAPE. Correlations for MR decreased with increasing distance from the sounding stations, suggesting causality with local air masses. In contrast to MR, both T and WS do not correlate with N and serve as statistical controls.

The results of this study are sufficient to predict thunderstorms in the Southwest, and particularly Langmuir Laboratory, but several modifications can be made in the original goals. Correlations for each type of lightning, CG and IC, should be compared to find discrepancies, as well as for comparison to prior studies that used NLDN data containing only CG flash counts. Large regional correlations should be analyzed for synoptic scale weather studies more applicable to the Midwestern U.S. All available years of LASA data other than 2005/2006 should be used to compare correlations from year-to-year. These additions will shed further light on the relationship between water vapor, convection, and flash counts, and improve the prediction of thunderstorms in areas other than the Southwest such as Oklahoma and Florida.

REFERENCES

Doswell, C. A. and Rasmussen, E. N. (1994). The Effect of Neglecting the Virtual Temperature Correction on CAPE Calculations. *Weather and Forecasting*, 9(4):625–629.

Energizer (2008). Energizer L522 Product Datasheet. Form No. EBC-4208E.

Farman, M. (1999). Universal Terminate Package for NSBF Balloon Operations. *American Institute of Aeronautics and Astronautics*, http://pdf.aiaa.org/preview/1999/PV1999_3864.pdf.

Garmin International (2006). GPS 15H and 15L Technical Specifications. Olathe, KS.

Garrabrant, B. (2008). Tinytrak SMT Owner's Addendum. www.byonics.com.

Hager, W., Sonnenfeld, R., Aslan, B., Battles, J., Lu, G., and Winn, W. (2007). Analysis of Charge Transport During Lightning Using Balloon Borne Electric Field Sensors and LMA. *Journal of Geophysical Research*, 112(D18):

Houze, R. A. (1993). *Cloud Dynamics*. Academic Press.

Jayaratne, E. R., Saunders, C. P. R., and Hallet, J. (1983). Laboratory Studies of the Charging of Soft-hail During Ice Crystal Interactions. *Quarterly Journal of the Royal Meteorological Society*, 109(461):609–630.

Krehbiel, P. (1986). *The Electrical Structure of Thunderstorms*, in *The Earth's Electrical Environment*. National Academy Press, Washington, D.C. pages 90-113.

Kuphaldt, T. R. (2007). Conductor and Insulator Tables *Fundamentals of Electrical Engineering and Electronics*, http://www.vias.org/feee/citable.html.

Lauritsen, D. K. (1991). Self Guided Recoverable Airborne Instrument Module. *Free Patents Online*, United States Patent 5186418, http://www.freepatentsonline.com/5186418.html.

Levanon, N., Afanasjevs, J., Ellington, S. D., Oehlkers, R. A., Suomi, V. E., Lichfield, E. W., Gray, M. W. (1975). The Twerle Balloon-to-Satellite Data Transmitting System. *IEEE Transactions on Geoscience Electronics*, GE-13(1).

Livingston, E. S., Nielsen-Gammon, J. W., and Orville, R. E. (1996). A Climatology, Synoptic Assessment, and Thermodynamic Evaluation for Cloud-to-Ground Lightning in Georgia: A Study for the 1996 Summer Olympics. *Bulletin of the American Meteorological Society*, 77(7):1483–1495.

Lucas, C., Zipser, E. J., and Lemone, M. A. (1994). Convective Available Potential Energy in the Environment of Oceanic and Continental Clouds: Correction and Comments. *Journal of the Atmospheric Sciences*, 51(24):3829-3830.

Marshall, T. C. and Rust, W. D. (1991). Electric Field Soundings Through Thunderstorms. *Journal of Geophysical Research*, 96(D12):22297–22306.

Meehan, J. (2002). Balloon v1.0. http://vpizza.org/ jmeehan/balloon/theidea.

Molinie, J. and Pontikis, C. A. (1995). A Climatological Study of Tropical Thunderstorm Clouds and Lightning Frequencies on the French Guyana Coast. *Geophysical Research Letters*, 22(9):1085–1088.

Office of the Federal Coordinator for Meteorology (1997). Federal Meteorological Handbook No. 3: Rawinsonde and Pibal Observations (FCM-H3-1997). Washington, D.C.

Orville, R. E. and Huffines, G. R. (2001). Cloud-to-Ground Lightning in the United States: NLDN Results in the First Decade, 1989-98. *Monthly Weather Review*, 129(5):1179-1193.

Parsch, A. (2006). Reconnaissance Balloons (WS-119L/WS-461L). *Directory of U.S. Military Rockets and Missiles Appendix 4: Undesignated Vehicles*, http://www.designation-systems. net/dusrm/app4/ws-119l.html.

Peterson, W. A., Christian, H. J., and Rutledge, S. A. (2005). TRMM Observations of the Global Relationship Between Ice Water Content and Lightning. *Geophysical Research Letters*, 32(14):L14819.

Qie, X., Toumi, R., and Yuan, T. (2003). Lightning Activities on the Tibetan Plateau as Observed by the Lightning Imaging Sensor. *Journal of Geophysical Research*, 108(D17):4551.

Raymond, D. and Wilkening, M. (1985). Characteristics of Mountain-Induced Thunderstorms and Cumulus Congestus Clouds from Budget Measurements. *Journal of the Atmospheric Sciences*, 42(8):773–783.

Shao, X., Stanley, M., Regan, A., Harlin, J., Pongratz, M., and Stock, M. (2006). Total Lightning Observations with the New and Improved Los Alamos Sferic Array (LASA). *Journal of Atmospheric and Ocean Technology*, 23:1273.

Smith, D. A., Eack, K. B., Harlin, J., Heavner, M. J., Jacobson, A. R., Massey, R. S., Shao, X. M., Wiens, K. C. (2002). The Los Alamos Sferic Array: A Research Tool for Lightning Investigations. *Journal of Geophysical Research*, 107(D13):4183.

Sonnenfeld, R., Battles, J., Lu, G., and Winn, W. (2006). Comparing E-field Changes Aloft to Lightning Mapping Data. *Journal of Geophysical Research*, 111(D20).

Stolzenburg, M., Rust, W. D., and Marshall, T. C. (1998). Electrical Structure in Thunderstorm Convective Regions 3. Synthesis. *Journal of Geophysical Research*, 103(D12):14097– 14108.

Takahashi, T. (1978). Riming Electrification as a Charge Generation Mechanism in Thunderstorms. *Journal of the Atmospheric Sciences*, 35(8):1536–1548.

Taylor, J. R. (1996). *An Introduction to Error Analysis: The Study of Uncertainties in Physical Measurements*. University Science Books, Sausalito, CA.

Vertex Standard (2003). VX-2R Operating Manual. Tokyo, Japan.

Williams, E. R. (1989). The Tripole Structure of Thunderstorms. *Journal of Geophysical Research*, 94(D11): 13151–13167.

Williams, E. R. and Renno, N. (1993). An Analysis of the Conditional Instability of the Tropical Atmosphere. *Monthly Weather Review*, 121(1): 21-36.

APPENDIX A

Glossary

APRS: Automatic Position Reporting System

CAPE: Convective available potential energy

CG: Cloud-to-ground

CONUS: Continental United States

DTMF: Dual-tone multi-frequency

E-Sonde: Electric field sonde

GPS: Global Positioning System

IC: Intra-cloud

IGRA: Integrated Global Radiosonde Archive

LASA: Los Alamos Sferic Array

LED: Light-emitting diode

LCL: Lifted condensation level

MR: Mixing ratio of water vapor to air

NCAR: National Center for Atmospheric Research

NLDN: National Lightning Detection Network

NSBF: National Scientific Balloon Facility

NWS: National Weather Service

N: Number of lightning flashes in 24 hours

PIC: Programmable intelligent computer

r: Correlation coefficient

SCR: Silicon-controlled rectifier

SWR: Standing wave ratio

T: Dry-bulb temperature

Tinytrak: Digital-to-audio encoder for APRS

TPW: Total precipitable water

TRMM: Tropical Rainfall Measuring Mission

TTL: Transistor-transistor logic

UTC: Coordinated universal time

WS: Wind speed

APPENDIX B

Parts Lists

Ref. No.	Part Name	Vendor (V) / Manufacturer (M)	Part No. (V and/or M)
1	GPS	Garmin (M)/GPS City (V)	15-H (V and M)
2	Tinytrak	Byonics (V,M)	SMT (V,M)
3	Radio	Yaisu (V,M)	VX-2 or VX-3 (V,M)
4	DTMF	Futurlec (V)	MT8870DE
5	PIC	Mouser (V)	579-PIC16F62804P (V)
6	SCR	Mouser (V)	511-X0402MF0AA2 (V)
7	9 V Battery	Energizer (M)	Alkaline (V)
8	Monofilament	High Catch	200 lb Test (V)
9	0.010” Aluminum	All-Foils (V,M)	5052-H34 (V,M)
10	Cake Pans	Parrish’s (V,M)	1” x 5”, 1” x 6” (V,M)
11	Aluminum	Metals (Alb.) (V,M)	6061-T6 (V,M)
12	LED	Mouser (V)	N/A
13	F/F Bulkhead	Mouser (V)	523-901-9209-A (V)
14	Rubber Grommet	Western Rubber (V,M)	(V,M)
15	Toggle Switch	Honeywell (V,M)	4TL1-3D (V,M)
16	4-40 All-thread	McMaster Carr (V)	
17	Plastic Spacers	McMaster Carr (V)	
18	AA Battery	Energizer (M)	Lithium (V)
19	9 V Battery	Energizer (M)	Lithium (V)
20	Acrylic Plate	New Mexico Tech (V,M)	N/A
21	555 Timer	Mouser (V)	595-SE555P (V)
22	13-bit Counter	Mouser (V)	595-CD4020BE (V)
23	Transistor	Mouser (V)	512-2N4401BU (V)
24	2-pin Connector (J1)	All Electronics (V,M)	CON-242P (V,M)
25	RG-174 SMA	Mouser (V)	530-415-0027-006 (V)
26	4-pin Connector (J10)	All Electronics (V,M)	CON-244 (V,M)
27	SMA M Adapter	Mouser (V)	530-142-0901-821 (V)

Table B.1: Parts List Referenced in Thesis

Ref.	Part Name	Vendor (V) / Manufacturer (M)	Part Number (V and/or M)
28	5 V Regulator	Digikey (V)	LP3963ES-5.0-ND (V)
29	33 μF Capacitor (C13)	Digikey (V)	P2029-ND (V)
30	68 μF Capacitor (U5)	Digikey (V)	478-1925-ND (V)
31	2-pin M Connector	All Electronics (V,M)	CON-210S (V,M)
32	2-pin F Connector	All Electronics (V,M)	CON-210P (V,M)
33	0.1 μF Capacitor (C3)	All Electronics (V,M)	RM-104 (V,M)
34	8-pin Dip (U2)	Mouser (V)	575-199308 (V)
35	16-pin Dip (U1)	Mouser (V)	575-199316 (V)
36	18-pin Dip (U4)	Mouser (V)	575-199318 (V)
37	0.47 μF Capacitor (C1)	Mouser (V)	74-199D35V0 (V)
38	5 μF Capacitor (C4)	Mouser (V)	75-TVA1303-E3 (V)
39	100 KΩ Resistor (R7)	Mouser (V)	273-100K-RC (V)
40	16 KΩ Resistor (R3)	Mouser (V)	273-16K-RC (V)
41	15 KΩ Resistor (R1)	Mouser (V)	273-15K-RC (V)
42	10 KΩ Resistor (R6)	Mouser (V)	273-10K-RC (V)
43	3.3 KΩ Resistor (R10)	Mouser (V)	273-3.3K-RC (V)
44	1 KΩ Resistor (R11)	Mouser (V)	273-1K-RC (V)
45	75 Ω Resistor (R12)	Mouser (V)	273-75-RC (V)
46	1 μF Capacitor (C8)	Mouser (V)	80-T350A105K035 (V)
47	22 pF Capacitor (C7)	Mouser (V)	140-500N5-220J-RC (V)
48	3.579 MHz Crystal (X1)	Mouser (V)	73-XT49U357-20 (V)
49	20.0 MHz Crystal (X2)	Mouser (V)	73-XT49U2000-20 (V)

Table B.2: Parts List Not Referenced in Thesis

APPENDIX C

Schematics of Instrument

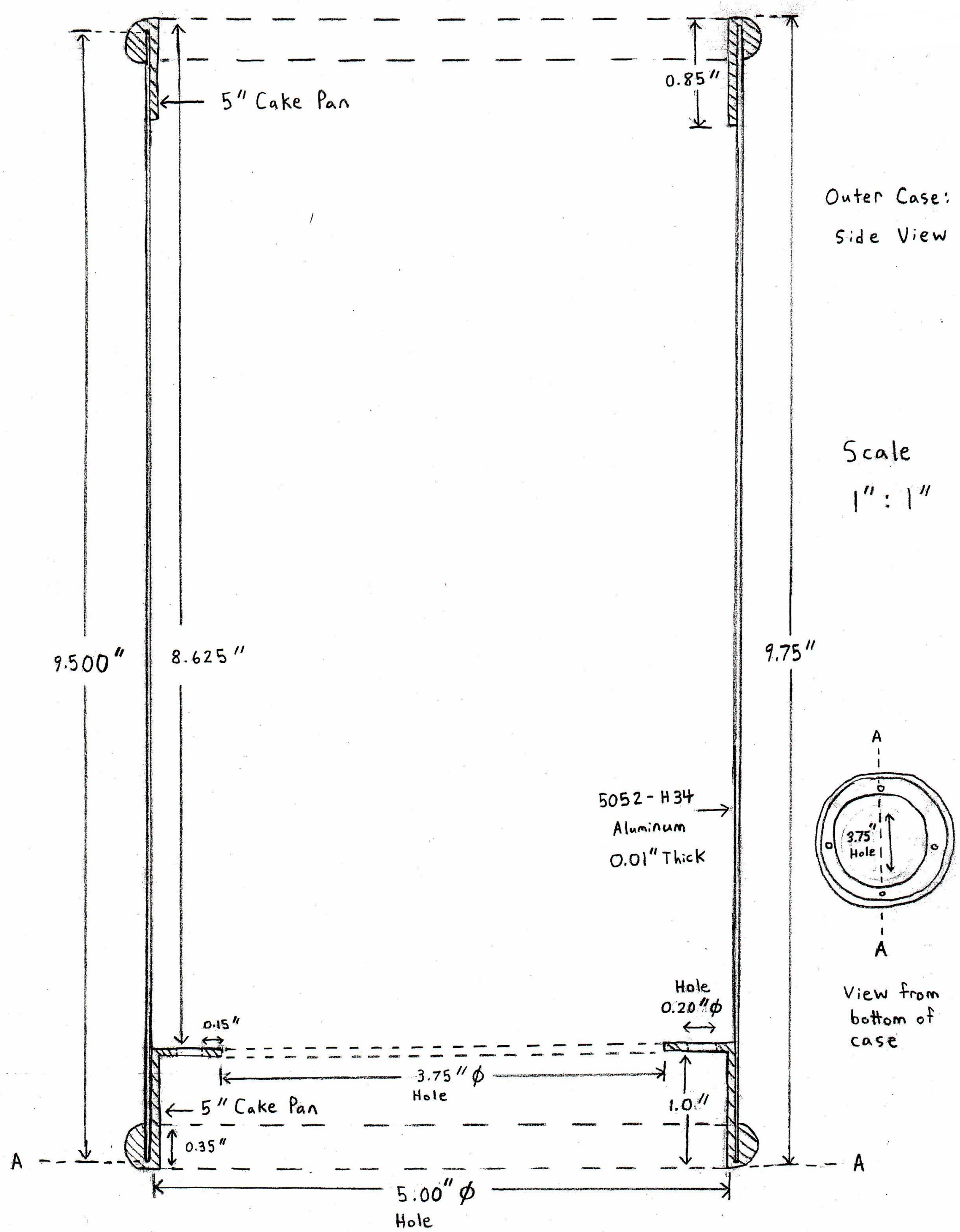

Figure C.1: Side Case

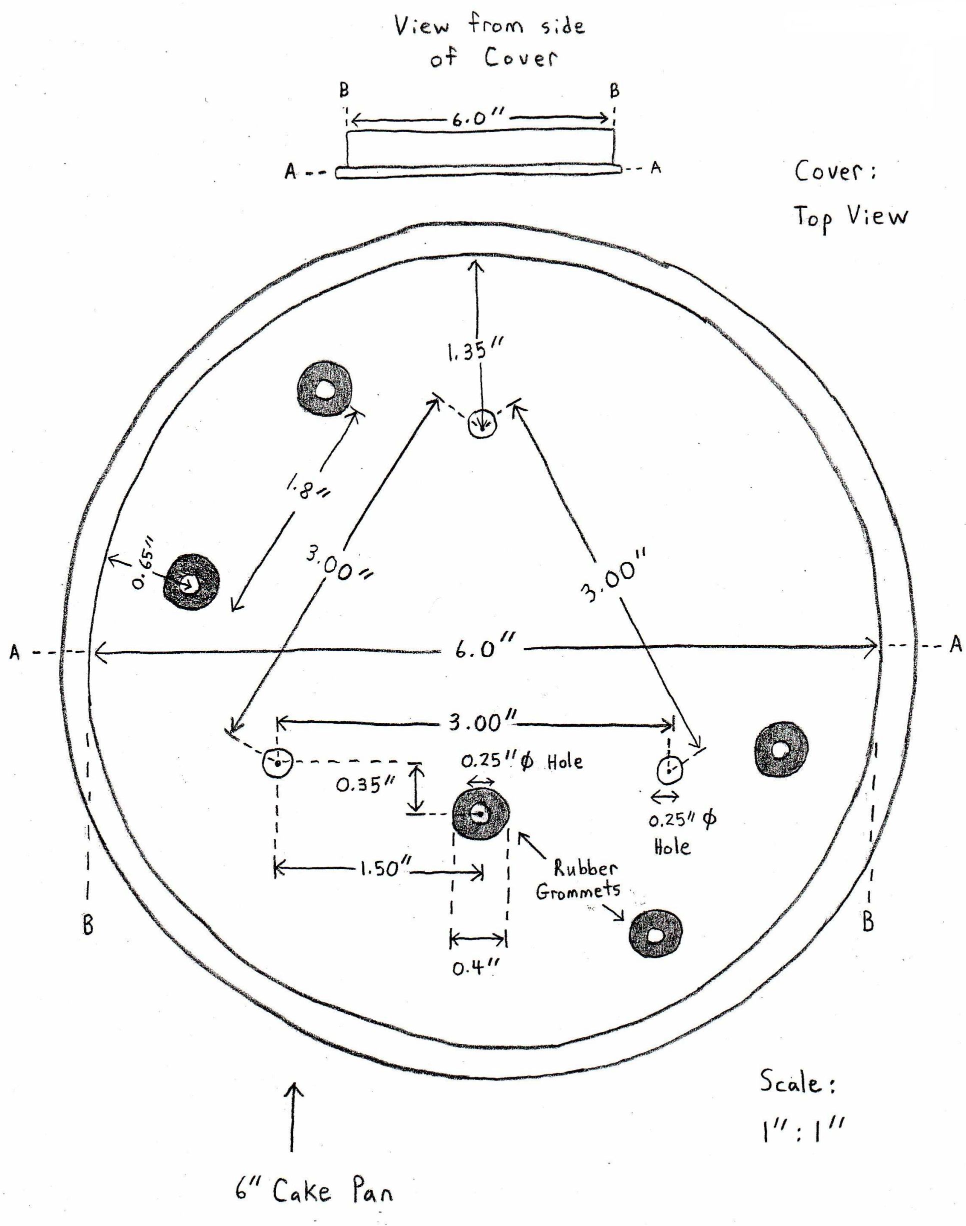

Figure C.2: Top

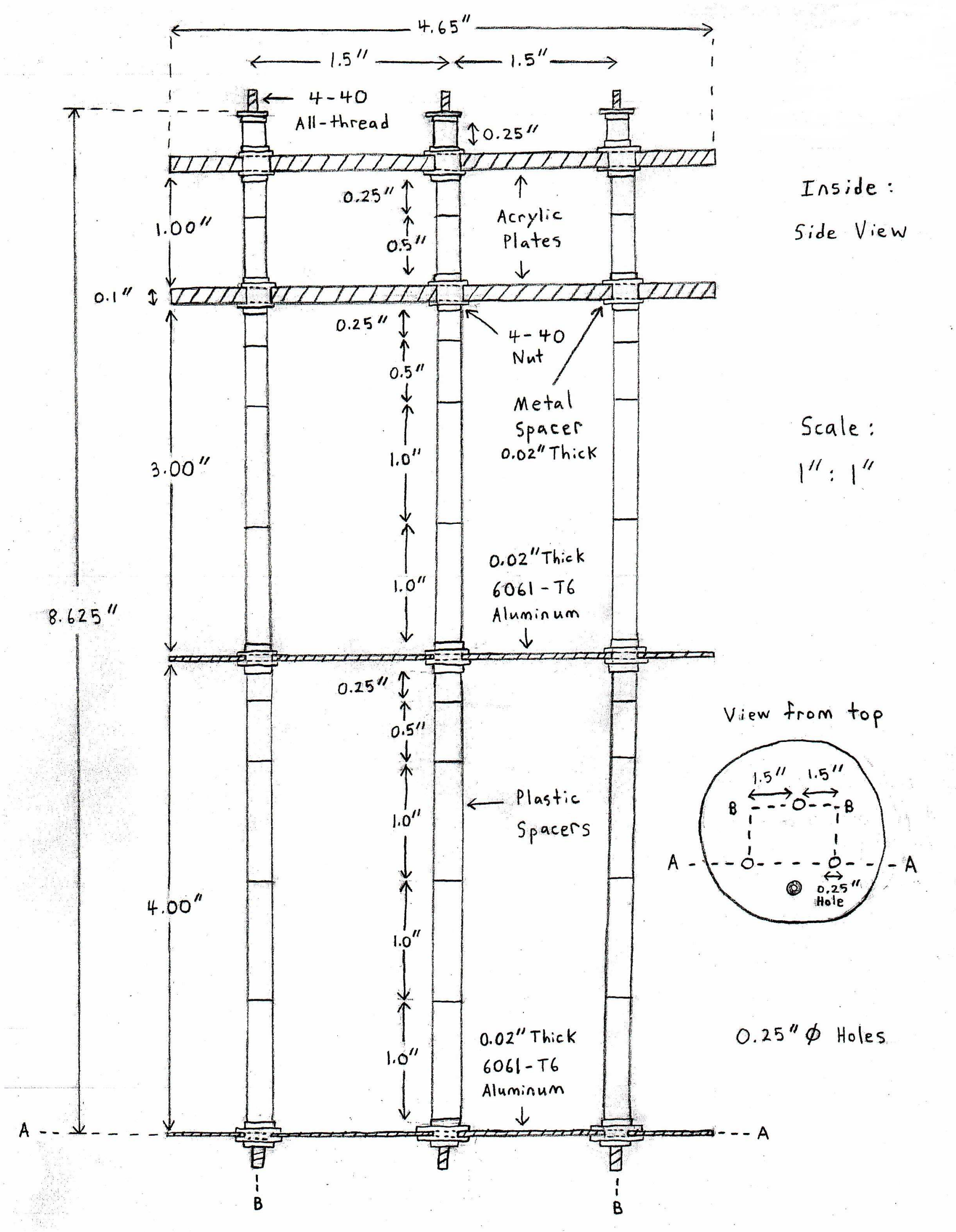

Figure C.3: Internal Posts

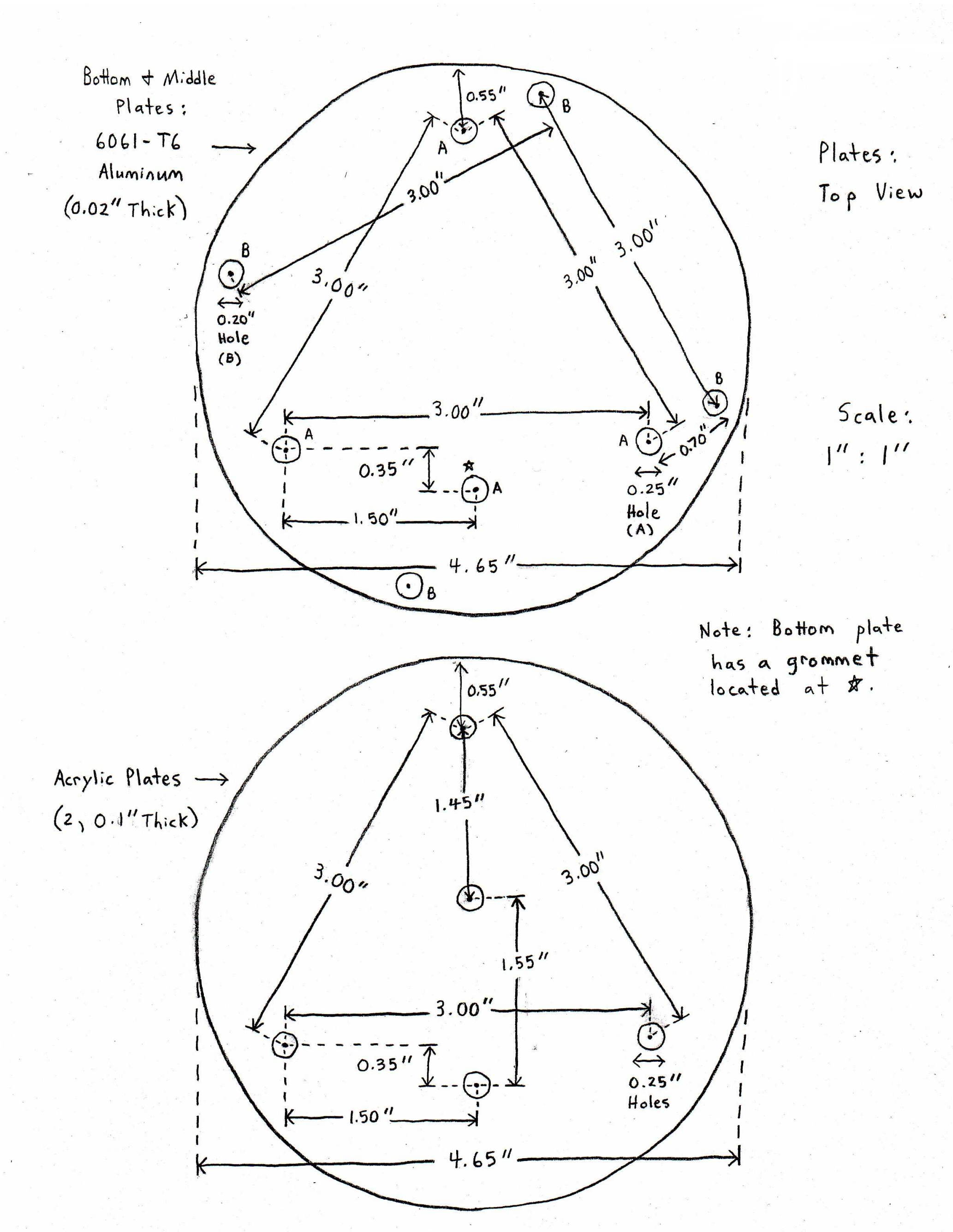

Figure C.4: Plates

APPENDIX D

Photos of Instrument and Parts

D.1 New Design

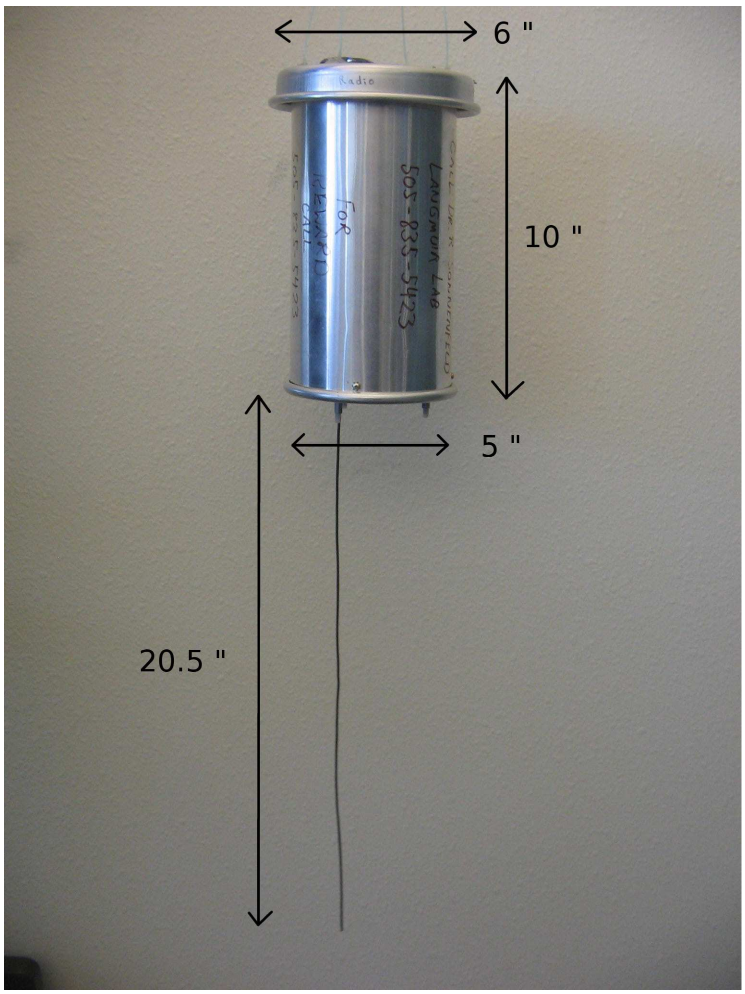

Figure D.1: External

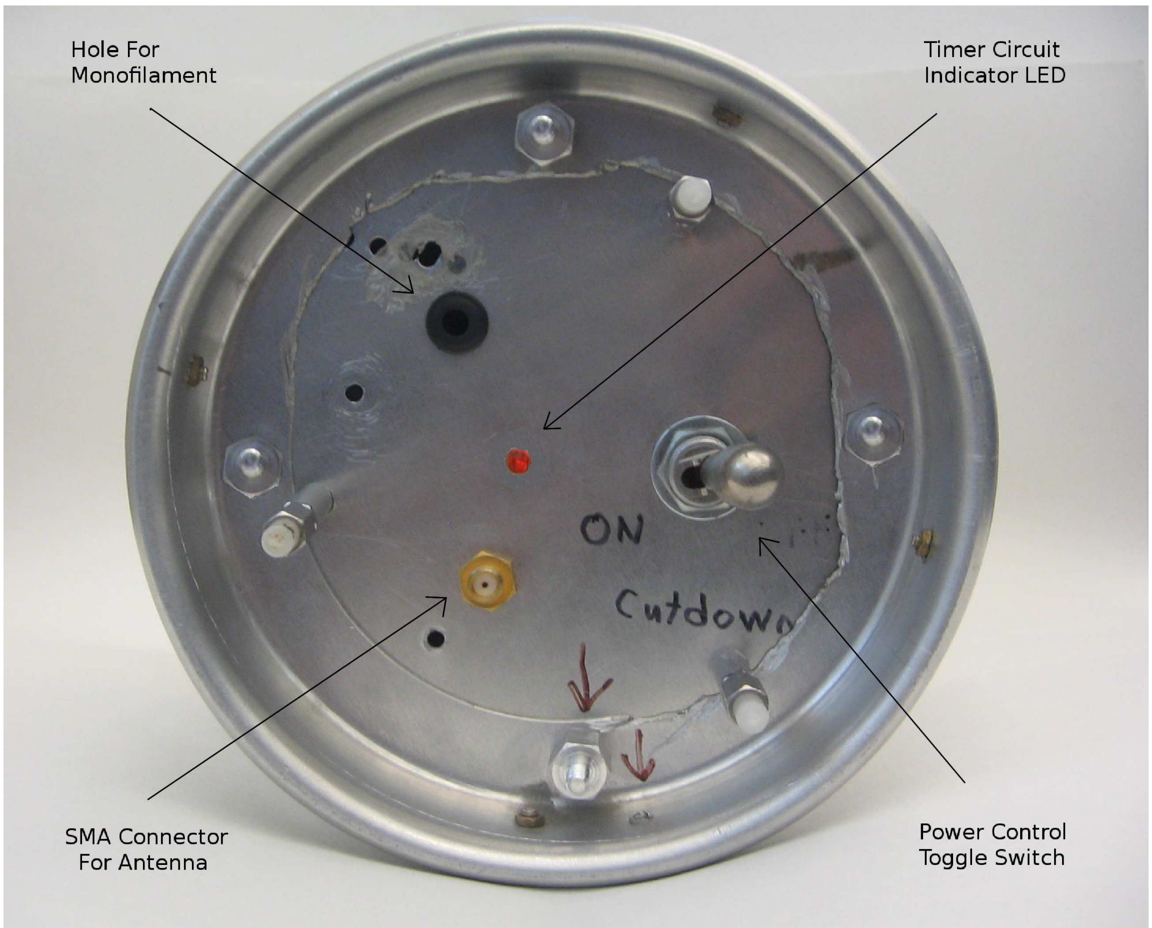

Figure D.2: Bottom

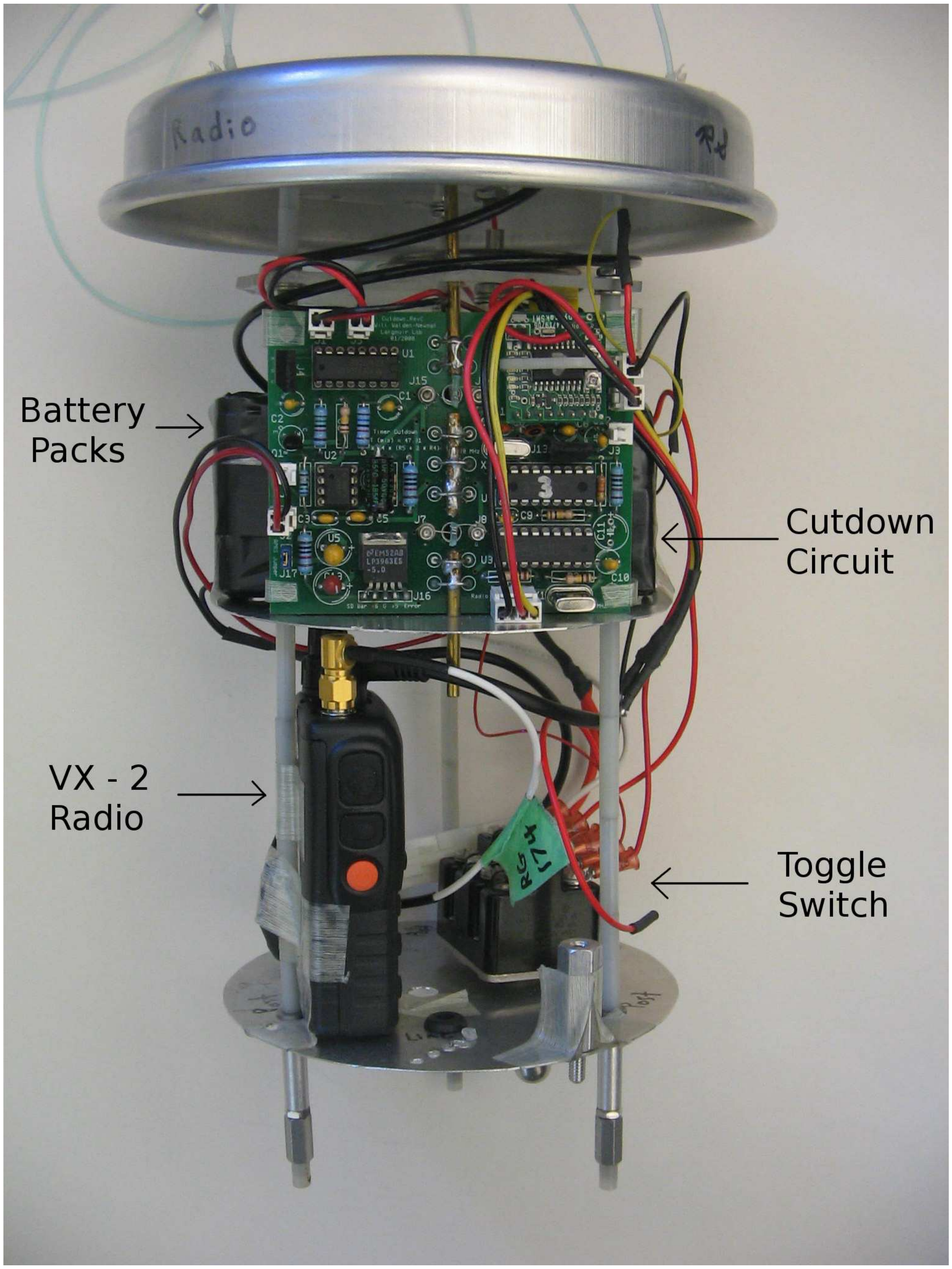

Figure D.3: Internal: Front View

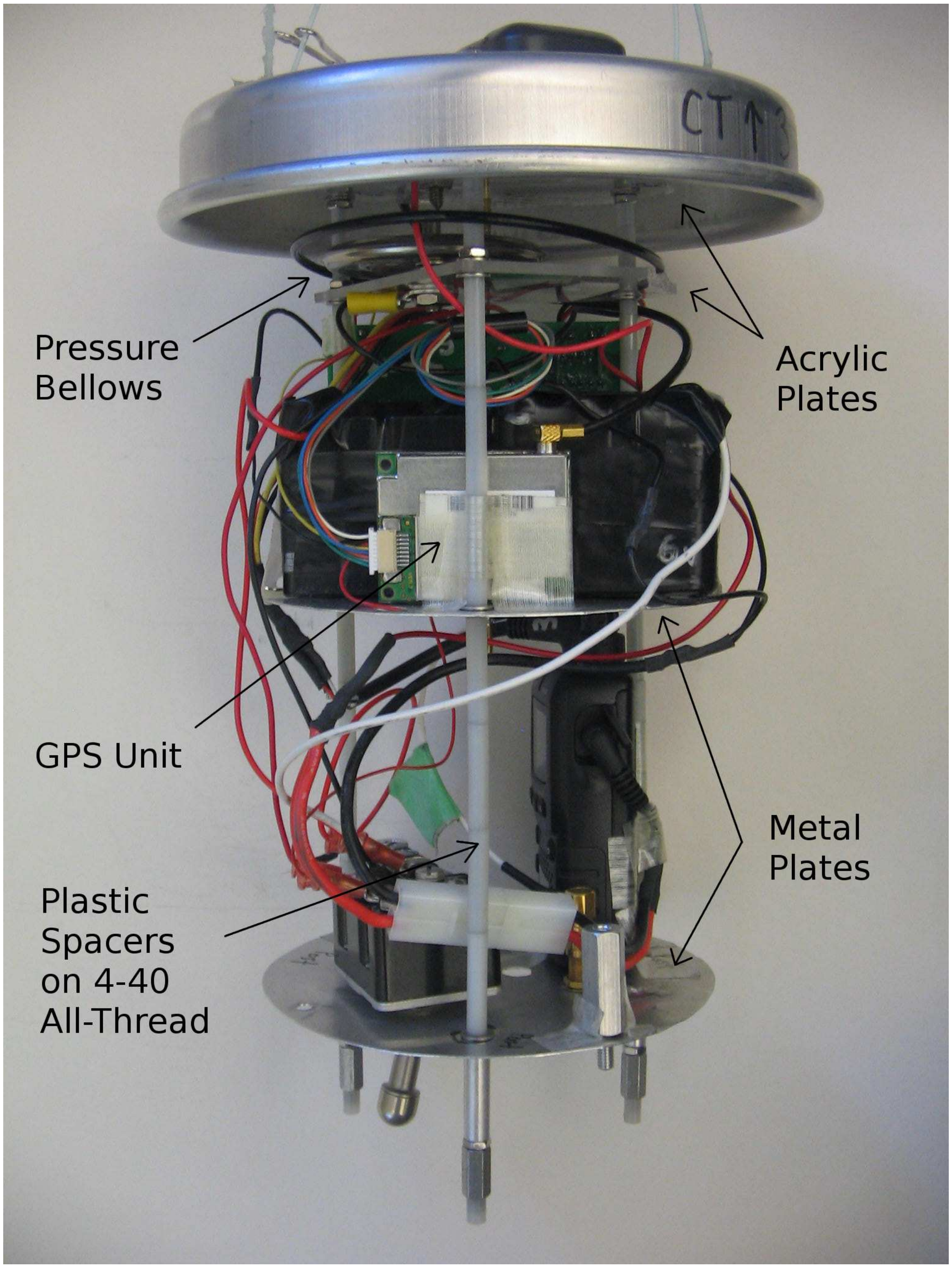

Figure D.4: Internal: Back View

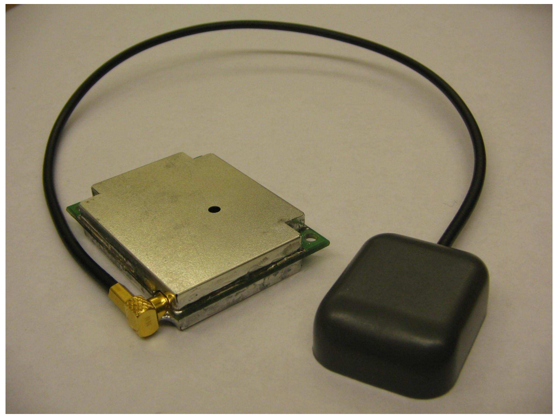

Figure D.5: GPS

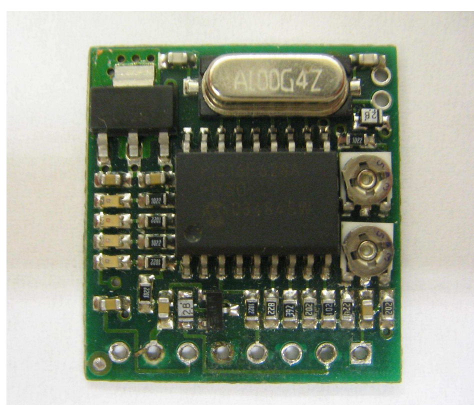

Figure D.6: Tinytrak

Figure D.7: VX-2 Radio

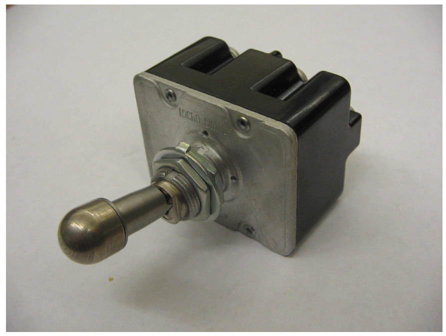

Figure D.8: Power Control Switch: View 1

Figure D.9: Power Control Switch: View 2

D.2 Old Design

Figure D.10: External

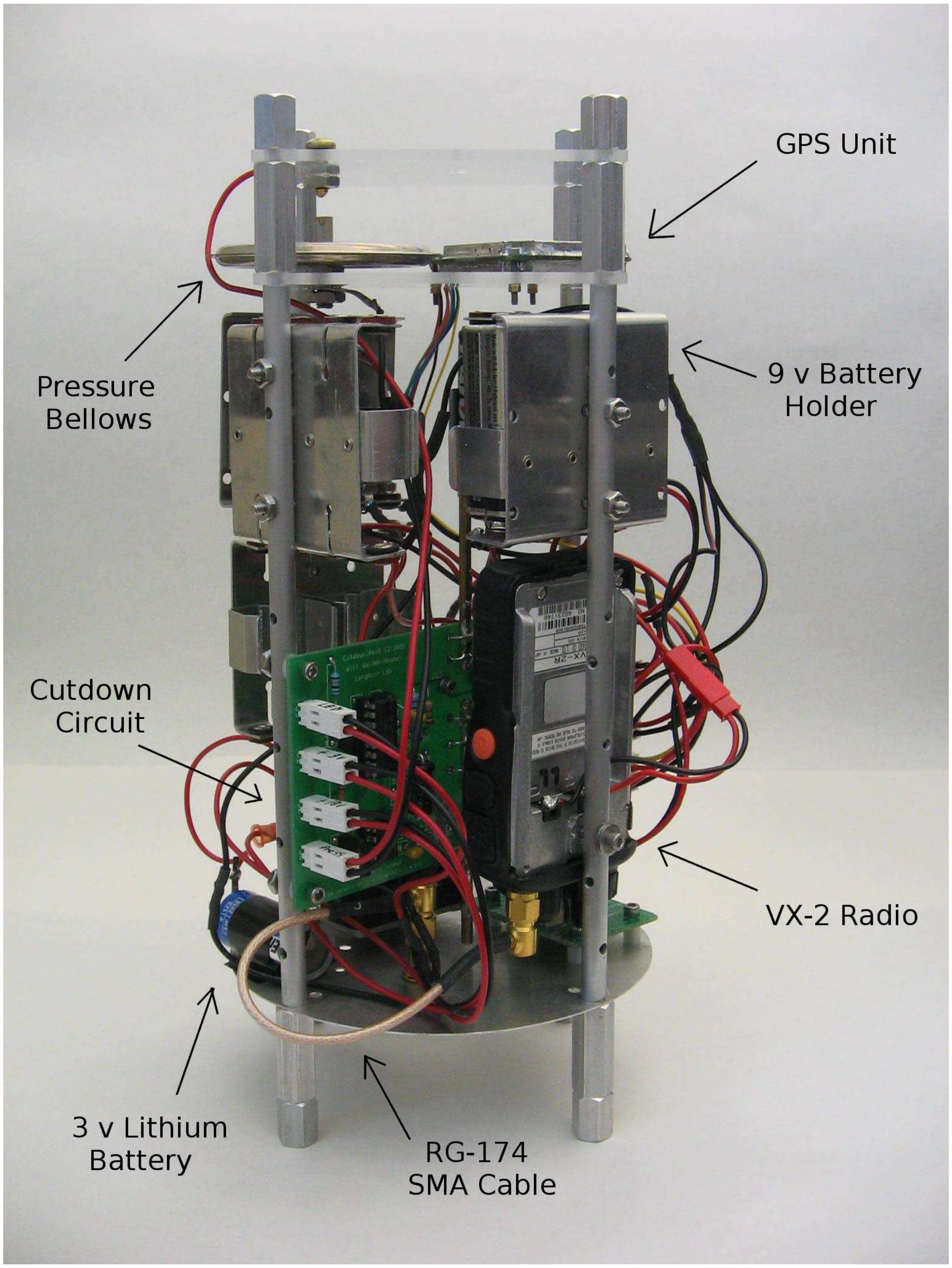

Figure D.11: Internal: View 1

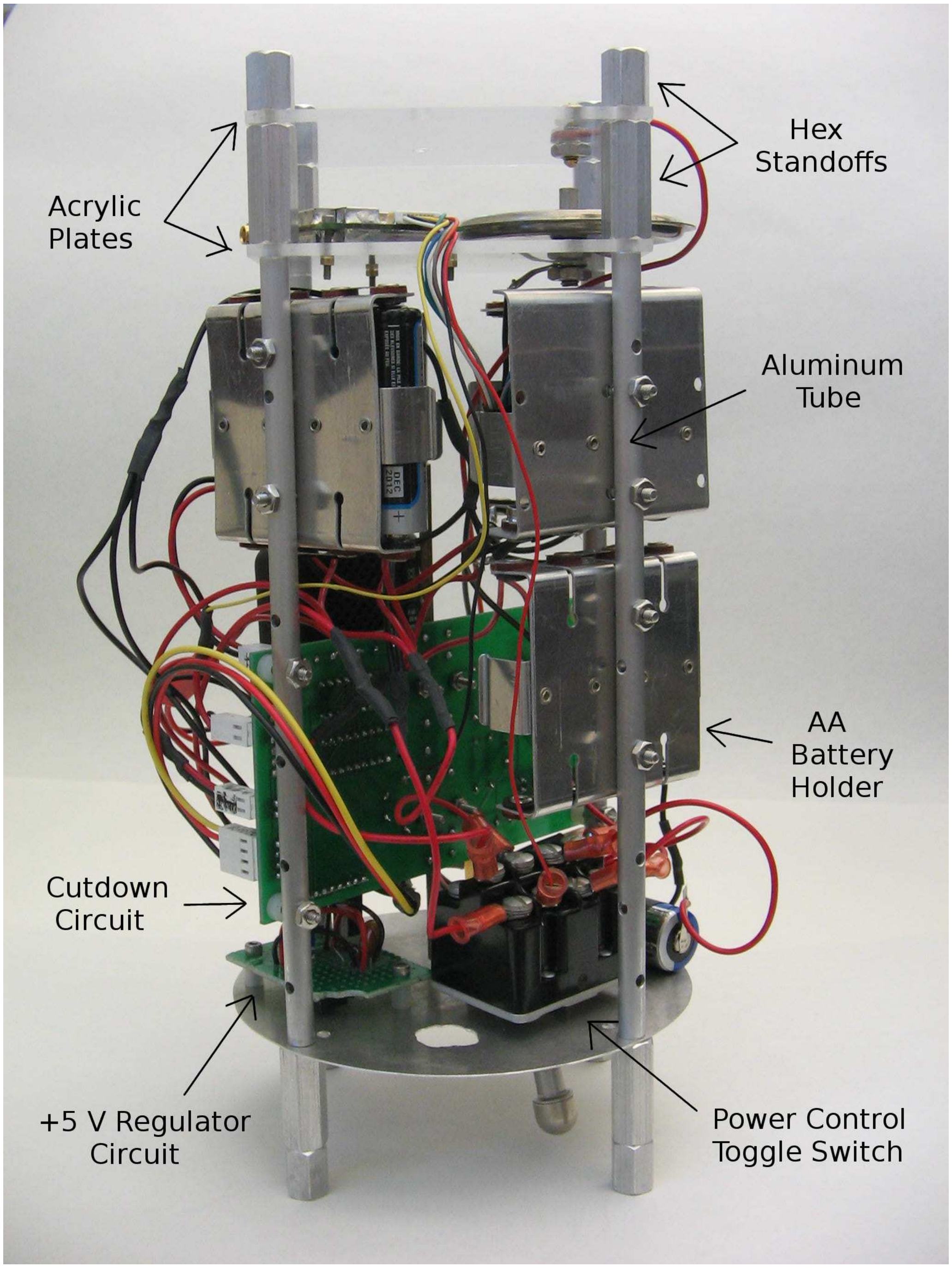

Figure D.12: Internal: View 2

APPENDIX E

Cut-down Circuit Schematic and Photos

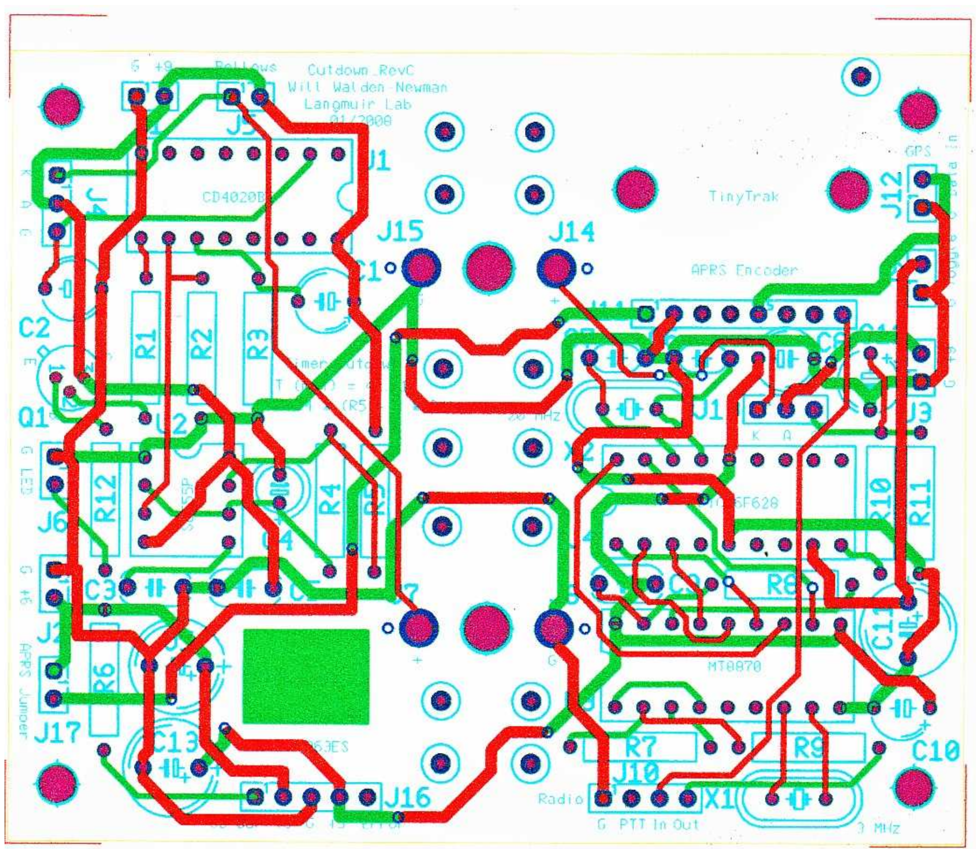

Figure E.1: Cut-down Circuit Layout: cutdown2.ewprj

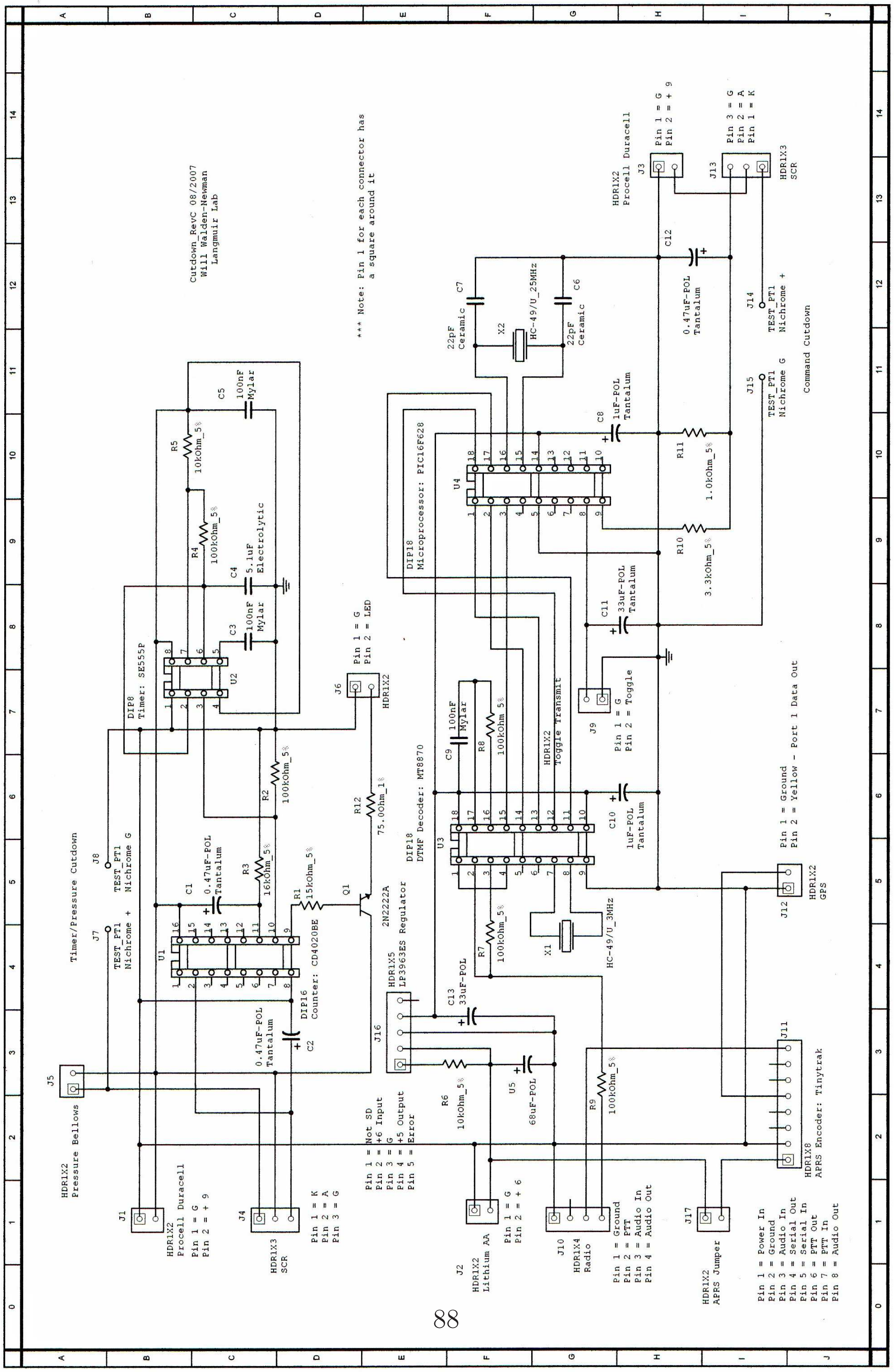

Figure E.2: Cut-down Circuit Schematic: cutdown2.ms7

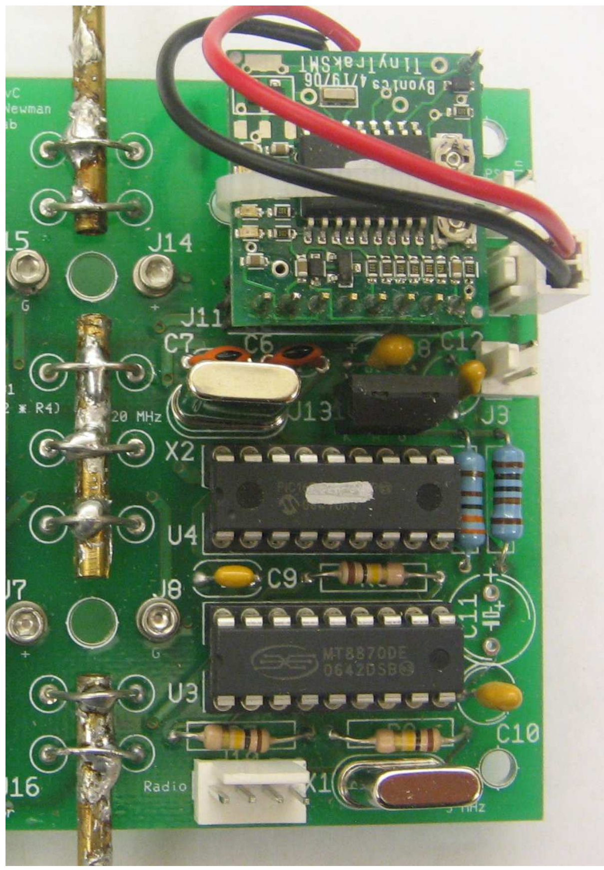

Figure E.3: Remote Cut-down Circuit

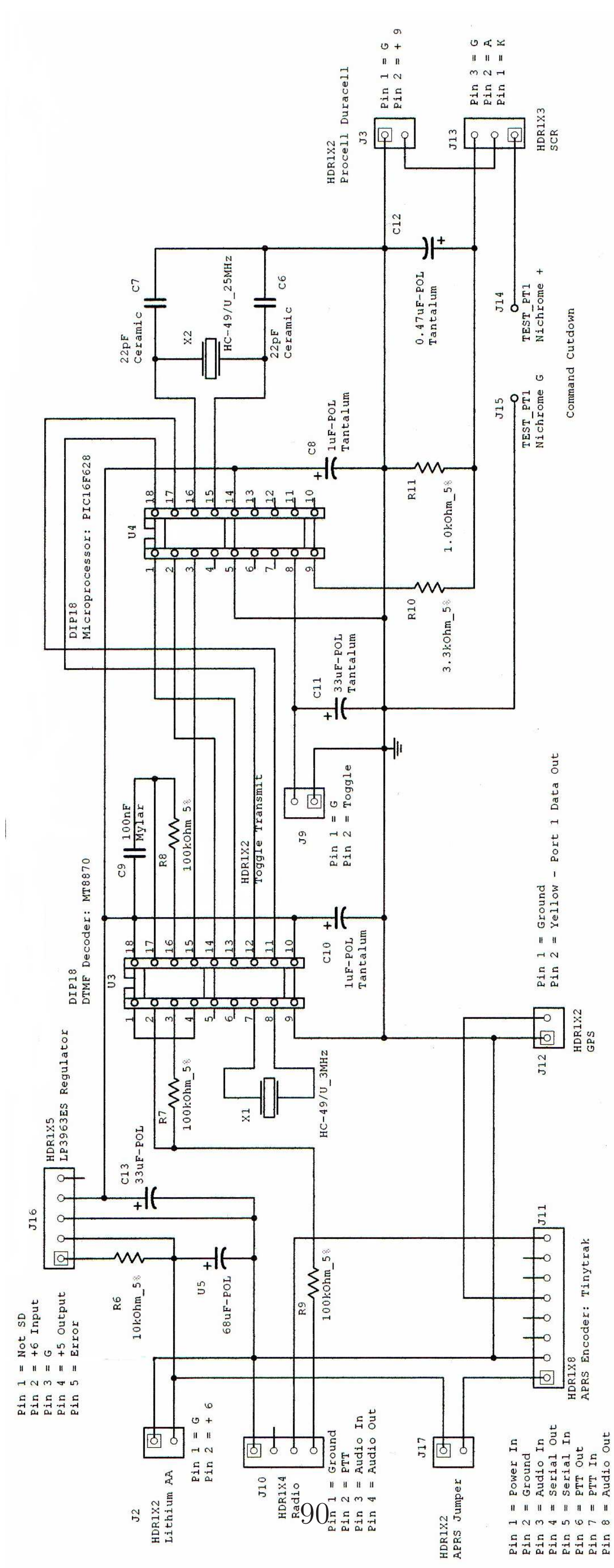

Figure E.4: Remote Cut-down Schematic

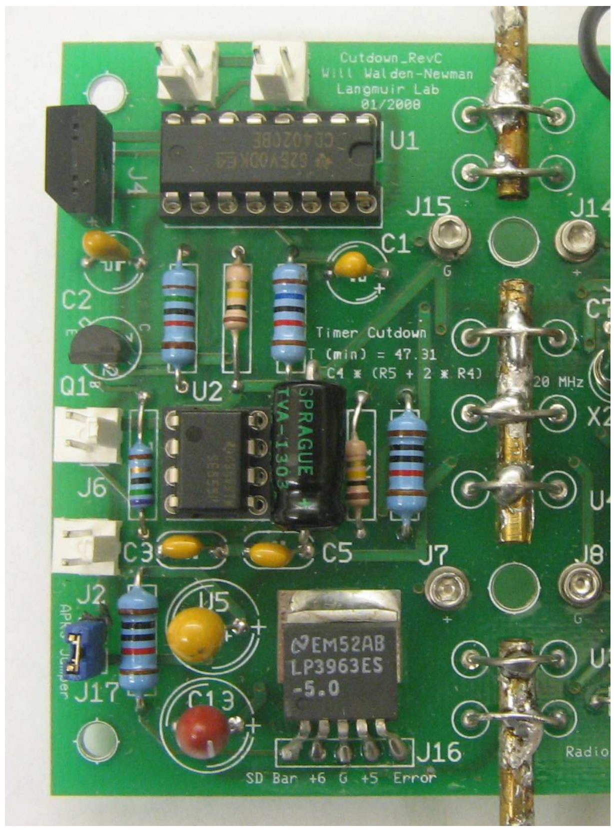

Figure E.5: Timer/Pressure Cut-down Circuit

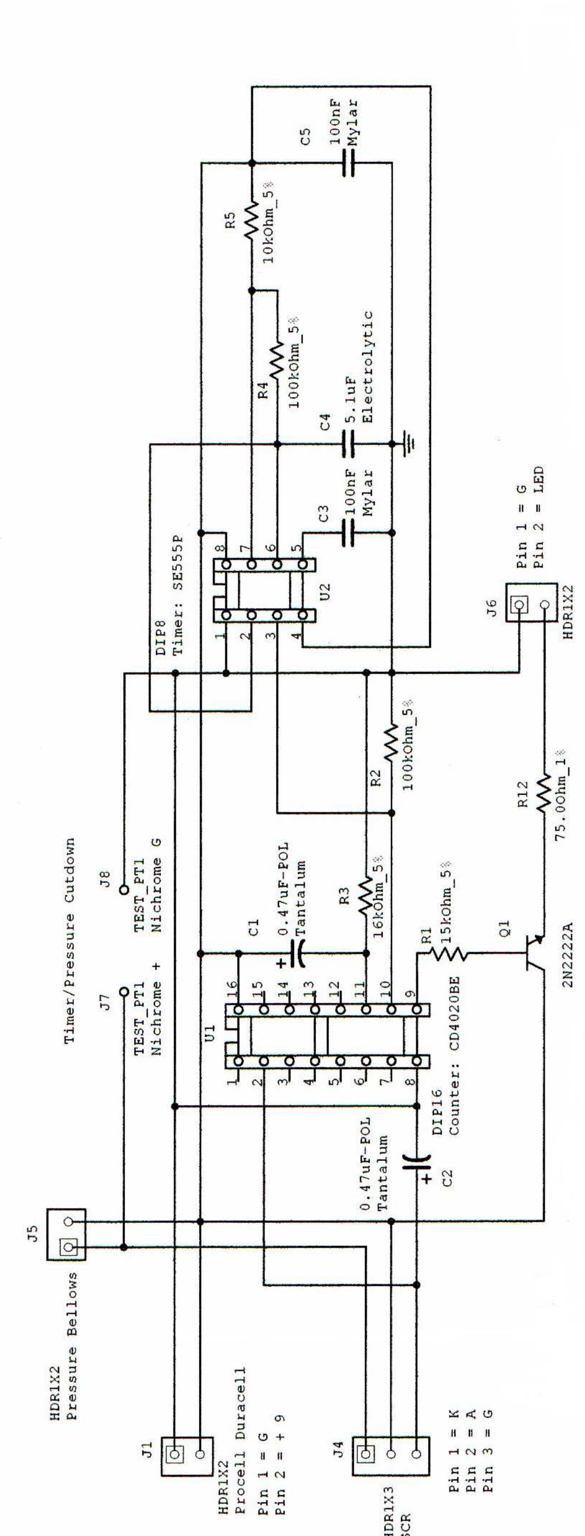

Figure E.6: Timer/Pressure Cut-down Schematic

APPENDIX F

Instructions for Programming Parts

F.1 VX-2

1. Set Channel 1 to receive at 148.95 MHz:
a. Use tuning dial to change frequency to 148.95 MHz.
b. Hold ’FW’ for a few seconds, until a blinking number appears at the top.
c. Use dial to change to channel 1, and press ’FW’ again to store it.

2. Program Ch.1 to transmit at 144.39 MHz:
a. Use tuning dial to change frequency to 144.39 MHz.
b. Hold ’FW’ again until a blinking number appears, and move dial to 1.
c. While holding ’PTT’, push ’FW’.

3. Lock radio into memory mode.
a. Power on the device while holding ’V/M’.
b. The radio should appear in Ch.1 with 148.95 MHz.
c. By pushing transmit, 144.39 MHz should appear.

4. Lock keyboard and tuning dial.
a. Exit memory mode, and then hold ’H/L’.
b. Move dial until ’LOCK’ appears, and then press ’H/L’.
c. Move dial until ’ALL’ appears, and then press ’PTT’ to save.
d. Press ’FW’ and then hold ’BAND’ to activate (or deactivate) locking.
e. Return to memory mode, and the radio is ready.

F.2 Tinytrak

Assign the following variables with corresponding values:

Callsign:KC5GTC-1X
where X = 0,1,2... is the instrument number

Digi Path: WIDE2-2

Symbol: O

Table/Overlay: /

Auto TX Delay: 333

Auto Transmit Rate: 120

Manual TX Delay: 73

Manual Transmit Rate: 2

Quiet Time: 1578

Calibration: 128

Text: Balloon Cutdown ? W07-01

Send Every: 2

Configure: COM1

Options to check: Send Altitude, Timestamp HMS

APPENDIX G

Code

G.1 Remote Cut-down with MicroC

```
// Code for Cut-down Instrument
// File: cutdownpackageX.c
//     where X = 1,..,4 is the instrument number

// Prototype Program for PIC processor control of
// of DTMF uplink commands. Initial system will
// remotely control cut-down

#define Tone0  10   // DTMF 0 symbol
#define Tone1  1    // DTMF 1 symbol
#define Tone2  2    // DTMF 2 symbol
#define Tone3  3    // DTMF 3 symbol
#define Tone4  4    // DTMF 4 symbol
#define Tone5  5    // DTMF 5 symbol
#define Tone6  6    // DTMF 6 symbol
#define Tone7  7    // DTMF 7 symbol
#define Tone8  8    // DTMF 8 symbol
#define Tone9  9    // DTMF 9 symbol
#define ToneA  13   // DTMF A symbol
#define ToneB  14   // DTMF B symbol
#define ToneC  15   // DTMF C symbol
#define ToneD  0    // DTMF D symbol
#define ToneP  12   // DTMF # symbol
#define ToneS  11   // DTMF * symbol

// Since 0 is valid for DTMF "D"
// do not use "D" as part of code

void main() {

        int DTMF0;
        int DTMF1;
        int DTMF2;
        int IN;
        int IN0;
```

```
        int IN1;
        int IN2;
        int IN3;
        int X;
        int TimeOut;

// Interface Specs from DTMF

        // IN0 = PORTA.F0
        // IN1 = PORTA.F1
        // IN2 = PORTA.F2
        // IN3 = PORTA.F3
        // VALID = PORTA.F4
        // TRIG = PORTB.F3
        // TRAN = PORTB.F2

// System Configuration

        CMCON = 0x07;   // Disable Comparator Mode
        TRISA = 0x1F;   // I/O Settings for PORT A
        TRISB = 0x00;   // Set PORT B as all Output

// Reset Variables

        DTMF0 = 0;      // Reset DTMF variables
        DTMF1 = 0;
        DTMF2 = 0;
        X = 0;          // Reset Position variable
        TimeOut = 0;    // Reset Timeout counter

        PORTA = 0;      // Initial Settings
        PORTB = 0x04;

        Delay_ms(1000);

// Cut-down Code Verification

        do
        {
                if (PORTA.F4)           // Check for VALID data
                {
                        Delay_us(1000);
                        IN = 0;         // Reset Input
                        IN0 = 0;
                        IN1 = 0;
                        IN2 = 0;
```

```
        IN3 = 0;
        if (PORTA.F0) IN0 = 1;          // Read DTMF data output
        if (PORTA.F1) IN1 = 1;
        if (PORTA.F2) IN2 = 1;
        if (PORTA.F3) IN3 = 1;
        IN = (1*IN0) + (2*IN1) + (4*IN2) + (8*IN3);  // Convert outputs to
        if (X == 0) DTMF0 = IN;                       // integer value
        if (X == 1) DTMF1 = IN;
        if (X == 2) DTMF2 = IN;
         ++X;                           // Increment position
        while (PORTA.F4)                // Wait for DV Flag to clear
                {
                        Delay_ms(1);
                }
}

if (X == 2)
{
        if (DTMF0 == ToneA && DTMF1 == Tone1)   // A1 Toggles transmit mode
        {
                PORTB = 0x00;
                Delay_ms(200);
                PORTB = 0x04;
                DTMF0 = 0;
                DTMF1 = 0;
                DTMF2 = 0;
                X = 0;
                TimeOut = 0;
        }
}

if (X > 0)
{
        Delay_ms(1);    // Count timer
        ++TimeOut;
}

if (TimeOut > 5000)     // Time out sequence
{
        TimeOut = 0;
        X = 0;
}

if (X == 3)
{
        if (DTMF0 == Tone1 && DTMF1 == Tone2 && DTMF2 == Tone3) //
```

```
                {
                        PORTB = 0x0C;       // Send trigger Command or TRIG = 1
                        Delay_ms(1000);
                        PORTB = 0x04;
                        DTMF0 = 0;          // Reset Variables
                        DTMF1 = 0;
                        DTMF2 = 0;
                        X = 0;
                        TimeOut = 0;
                }
                else
                {
                        DTMF0 = 0;
                        DTMF1 = 0;
                        DTMF2 = 0;
                        X = 0;
                        TimeOut = 0;
                }
        }
    } while(1);
}
```

G.2 MR Calculation with Matlab

```
% Load data file from IGRA sounding:
% http://www.ncdc.noaa.gov/oa/climate/igra/index.php

load('/filelocation/sounding.mat');

% Define Constants
T0 = 273.15; % K, Reference Temperature
es0 = 611; % Pa, Reference Vapor Pressure
Lv = 2.25e6; % J/K*kg, Latent Heat of Vaporization
Rv = 461.5; % J/K*kg, Gas Constant for water vapor

% Define Temperature (T) and Dew Point Depression (DPD)
% Note: Data had x 10 factor
T = (1./10).*sounding(:,4) + 273.15;
DPD = (1./10).*sounding(:,5);

% Define P in pascals
P = sounding(:,2);

% Find Dew Point Temperature (Td) from DPD
Td = T - DPD;
```

```
% Find Vapor Pressure (e) from Td
e = es0.*exp((Lv./Rv).*((1./T0) - (1./Td))); % Pa

% Find Mixing Ratio (w) from e and P
w = ((0.622).*e)./(P - e);

% Convert w from kg/kg to g/kg
w = 1000.*w;
```

G.3 CAPE Calculation with Matlab

```
% Calculation assumes mean mixed layer CAPE
% from the first 500 meters

% Does not include virtual temperature correction,
% which could explain high errors at small CAPE.

% Load data file from UW sounding page:
% http://weather.uwyo.edu/upperair/sounding.html

load('/filelocation/sounding.mat');

% Define Constants
g = 9.8; % m/s^2
dT = 0.0098; % K/m, Dry Adiabatic Lapse Rate
cpd = 1004; % J/K*kg, Specific heat at dry air
Lv = 2.25e6; % J/K*kg, Latent Heat of Vaporization
Rd = 287; % J/K*kg, Gas Constant for dry air
e = 0.622; % Rd/Rv, Ratio of gas constants

% Definitions of Columns

% Column 1: Pressure (P) in Pa
P(:,1) = 100.*sounding(:,1);

% Column 2: Height (H) in m
H(:,1) = sounding(:,2);

% Column 3: Temperature (T) in k
T(:,1) = sounding(:,3) + 273.15;

% Column 4: Dewpoint Temperature (DP) in K
DP(:,1) = sounding(:,4) + 273.15;
```

```
% Column 5: Relative Humidity(RH) in %
RH(:,1) = sounding(:,5);

% Column 6: Mixing Ratio (MR) in kg/kg
MR(:,1) = (10^(-3)).*sounding(:,6);

% Column 9: Potential Temperature (TA) in K
TA(:,1) = sounding(:,9);

% Column 10: Equivalent Potential Temperature (TE) in K
TE(:,1) = sounding(:,10);

% Column 11: Virtual Potential Temperature (TV) in K
TV(:,1) = sounding(:,11);

% Define Poisson Constant for Moist Air
k = 0.2854.*(1 - 0.24.*MR(:,1));

% Find average values from below 500 m:
% Assumes data file has 100 rows
n = 2;
m = 2;
Tadd = T(1,1);
Padd = P(1,1);
DPadd = DP(1,1);
kadd = k(1,1);
TAadd = TA(1,1);
TEadd = TE(1,1);
MRadd = MR(1,1);
deltaH = H(:,1) - H(1,1);
for n=2:100;
    if deltaH(n,1) <= 500;
        Tadd = Tadd + T(n,1);
        Padd = Padd + P(n,1);
        DPadd = DPadd + DP(n,1);
        kadd = kadd + k(n,1);
        TAadd = TAadd + TA(n,1);
        TEadd = TEadd + TE(n,1);
        MRadd = MRadd + MR(n,1);
        n = n+1;
        m = m+1;
    else
        n = 100;
    end;
end;
Tave = (1/(m-1)).*sum(Tadd);
```

```
Pave = (1/(m-1)).*sum(Padd);
DPave = (1/(m-1)).*sum(DPadd);
kave = (1/(m-1)).*sum(kadd);
TAave = (1/(m-1)).*sum(TAadd);
TEave = (1/(m-1)).*sum(TEadd);
MRave = (1/(m-1)).*sum(MRadd);

% Find T (LCLT) and P (LCLP) at
% the Liquid Condensation Level (LCL)
LCLT = (1/((1/(DPave-56)) + (1/800)*log(Tave/DPave))) + 56;
LCLP = Pave.*(LCLT/Tave)^(1/kave);

% Find the LCL (in Pa)
n = 1;
m = 1;
for n=1:100;
    if P(n,1) > LCLP;
        n = n+1;
        m = m+1;
    else
        n = 100;
    end;
end;
j = m-1;
LCL = P(j,1);

% Find the Equivalent Potential Temperature at the
% LCL, or the Moist Adiabat (EPT and EPTave)
EPT = (T(j,1) + (Lv/cpd)*MR(j,1))*(100000/P(j,1))^(Rd/cpd);
EPTave = (Tave + (Lv/cpd)*MRave)*(100000/Pave)^(Rd/cpd);

% Find T of parcel raised dry adiabatically (TP) to LCL
TP(1,1) = T(1,1);
n = 2;
for n=2:j;
    TP(n,1) = T(n-1,1) - dT.*(H(n,1)-H(n-1,1));
    n = n+1;
end;

% Find T of parcel raised moist adiabatically onward
i = j+1;
for n=i:100;
    TP(n,1) = EPT.*(P(n,1)./100000).^(Rd/cpd) - (Lv/cpd).*MR(n,1);
    n = n+1;
end;
```

```
% Sum CAPE at heights where TP > T

% Note: It is not known what type of summing is chosen
% at the sounding website. Thus, values calculated are
% near the actual values but do not match. However, since
% both values are similar, I can assume the CAPE values
% posted at UW and used in this study are valid.

CAPE = 0;
n = 2;
m = n-1;
for n=2:100;
    if TP(n,1) > T(n,1);
        CAPE = CAPE + g.*(H(n,1) - H(n-1,1)).*(1./T(n,1)).*(TP(n,1)-T(n,1));
        n = n+1;
    else
        n = n+1;
    end;
end;

Example Calculations:
Link to files: http://weather.uwyo.edu/upperair/sounding.html

% Sounding: Alb. July 4th 12Z
% Actual CAPE = 985.20, Calculated CAPE = 1067.63

% Sounding 2: Alb. July 5th 12Z
% Actual CAPE = 38.17 Calculated CAPE = 1.08

% Sounding 3: Alb. June 17th 00Z
% Actual CAPE = 527.44, Calculated CAPE = 674.38
```

APPENDIX H

Range Test Results

Time (UTC)	Long. (Deg., Min.)	Lat. (Deg., Min.)	Loc. Description
20:50:13	106, 53.68	34, 1.83	Socorro Airport
20:56:17	106, 53.04	33, 58.73	N/A
21:06:43	106, 52.13	33, 55.28	San Antonio, NM
21:31:20	106, 53.38	33, 48.35	N/A
22:23:34	106, 49.56	33, 54.76	N/A
22:40:26	106, 45.24	33, 53.53	N/A
22:52:31	106, 42.10	33, 53.15	16 miles SE of Socorro
23:12:47	106, 32.46	33, 52.71	23 miles SE of Socorro
23:26:54	106, 28.16	33, 52.67	31.4 miles from Repeater

Table H.1: Transmission Range Test